

Contents lists available at ScienceDirect

Polymer

journal homepage: www.elsevier.com/locate/polymer





Building a phenomenological chain-level understanding of mechanics of semicrystalline polymers: 2. Conceptual

Shi-Qing Wang*, Travis Smith, Chaitanya Gupta, Asal Y. Siavoshani

School of Polymer Science and Polymer Engineering, University of Akron, Akron, OH, 44325, USA

ABSTRACT

To rationalize the comprehensive phenomenology in Paper 1 (this volume, p. 125878), we present a qualitative description for the mechanical behavior of semi-crystalline polymers (SCPs) through a synthesis of prior understandings about the mechanical characteristics of glassy and semicrystalline polymers. Based on the central idea to regard an SCP as a crystalline chain network (CCN), in which a test chain can have crystalline and amorphous strands, we emphasize several key concepts: (a) crystallization determines the structure of the CCN, which is generally weaker than the pre-crystallization chain network in the molten state formed by interchain uncrossability, (b) ductility in SCPs is afforded by a sufficiently robust CCN, and (c) yielding and plastic deformation of SCPs require a successful structural transformation involving shape-change of crystalline phases through appreciable chain pull-out from the crystalline phases without breakdown of the CCN. In other words, it is the CCN that drives ductile SCPs to undergo yielding and subsequent large deformation through massive pull-out of load bearing strands (LBSs), which are the it and entangling strands. Brittle fracture and lack of drawability occur in those SCPs where the CCN is too weak (due to a sparse population of LBSs) to cause sufficient meltdown of crystalline phases: There are not enough LBSs to undergo pull-out that is necessary for yielding and crystal transformation. Based on these concepts we can explore the processing-structure-property (P–S–P) relationship by demonstrating how pre-deformation in either crystalline or molten state produces more favorable structures for stronger mechanical characteristics.

1. Introduction

Several hundred million tons of polymers are consumed because of their adequate mechanical properties [1-3]. To make more efficient and effective use of these materials, the chain-level study of polymer mechanics should be a highly valuable and central topic in polymer science. With the recent development in understanding the molecular mechanism of ductility in glassy non-crystalline polymers [4,5], it has become possible to address the additional complication arising from crystallization. Since a majority of polymers are semicrystalline, there is a greater need to develop a clear molecular picture to rationalize the mechanical behavior of SCPs over a wide temperature range, i.e., both above and below Tg. The present Paper 2 attempts to meet this need to some degree. We note at the onset that the content of this paper draws heavily from the experimental phenomenology summarized in Paper 1 (this volume, p. 125878). While SCPs under the experimental study have broad molecular weight distribution, our theoretical discussion ignore effects of polydispersity and only considers the condition of high molecular weight, as even PE cannot remain ductile at low molecular weight [6]. As recently demonstrated [7], low molecular weight leads to reduced tie molecule content and loss of ductility, as expected [8].

Although the mechanical behavior of polymers is a core subject in

polymer science and engineering, the current state-of-the-art is highly unsatisfactory. Thanks to the adequate mechanical properties of polyolefins (PE and PP), which are 60% of all polymers, it was not necessary to figure out why PE and PP possess such desirable mechanical characteristics until the poor mechanical characteristics of two sustainable polymers, PHA and PLLA, challenged us to search for the means to improve ductility in certain SCPs. Given the structural complexity of SCPs and elusive crystallization processes, it has so far been rather intractable to obtain any chain-level description for the mechanical behavior of SCPs.

SCPs of high molecular weight above T_g are like any yield-stress materials, unable to undergo plastic flow below a threshold stress (cf. Section 3.1.1 in Paper 1 (this volume, p. 125878)). Crystals effectively act like crosslinks, enabling SCPs to resist failure. Regarding the mechanical responses of rubbery SCPs (above T_g), the central question is how such SCPs acquire high strength and avoid brittle fracture. It is known that sufficient crystallization can even make PE brittle [9]. Moreover, SCPs are nearly never ductile below T_g where they face additional obstacles due to vitrification. The mission of the present study is to look for a useful picture along with instructive concepts and proper language that can rationalize the experimental observations. Specifically, in this Paper 2 we will discuss the structure-(mechanical)

E-mail address: swang@uakron.edu (S.-Q. Wang).

^{*} Corresponding author.

property relationship to pave the road toward establishment of the P–S–P. To do so, two key concepts are discussed in detail: yielding and drawability, or lack of it. In addition, this paper attempts to define the various basic concepts in detail such as whitening, ductility, predrawing and pre-melt stretching, mechanical melting.

Specifically, Paper 2 is organized as follows. Sections 2 presents a speculative description of the hierarchical structures of SCPs of high molecular weight. The structural relationship between crystalline and amorphous phases is discussed through the phenomenon of various types of stress-induced whitening (cavitation) in Section 3. In Section 4 we suggest a scaling expression to relate Young's modulus to the network structure. Section 5 is on the concept of yielding; we will discuss different explanations concerning structural changes that result in yielding, including fragmentation [10], melting [11], and slip [12]. Section 6 is an essential part of this paper, explaining temperature dependence of ductility in rubbery SCPs. Normal and anomalous rate dependences of ductility/drawability are discussed in Section 7. Section 8 is another key part of the present work, relating the lack of *drawability* to low LBS density. Section 9 discusses the mechanical responses of SCPs below their Tg. Sections 10 and 11 may be regarded as theoretical predictions based on the available phenomenological understanding that was reviewed in the preceding Sections 2 to 9. They demonstrate the benefits of pre-deformation in either crystalline (predrawing) or molten state (pre-melt stretching). Such pre-deformation can turn brittle SCPs into tough and ductile materials. As an extension of the study of the predrawing effect in Section 10, Section 12 indicates the phenomenon of *mechanical melting* in predrawn SCPs upon annealing above the pre-deformation temperature. Paper 2 accompanies Paper 1 (this volume, p. 125878) in the sense that all phenomena presented in Paper 1 are correspondingly discussed in Paper 2 according to Table 1 in Paper 1, which also contains a list of abbreviations common to both Paper 1 and Paper 2.

2. Hierarchical structures and underlying chain network

Isothermal melt crystallization in quiescence usually results in a spherulitic morphology. With increasing crystallinity, rigid spherulites become space filling, as shown by the polarized-optical microscopic (POM) photo in Fig. 1(a) where the interspherulitic boundaries are traced by red and white lines (color online) in Fig. 1(b) on the same scale. Here spherulites are assemblies of stiff lamellae, as depicted in Fig. 1(c). Because lamellae are jammed up within spherulites, intact spherulites may be regarded as rigid. At sufficiently high crystallinity, an SCP has high Young's modulus E when spherulites impinge on one another to fill up space, as shown in Fig. 1(b). The amorphous regions between spherulites may look like the sketch in Fig. 1(d). The interspherulitic regions may be different from the amorphous regions inside a spherulite, but Fig. 1(d) does not encompass more details to describe any difference.

SCPs are often regarded as "composites" [14,15], with spherulites

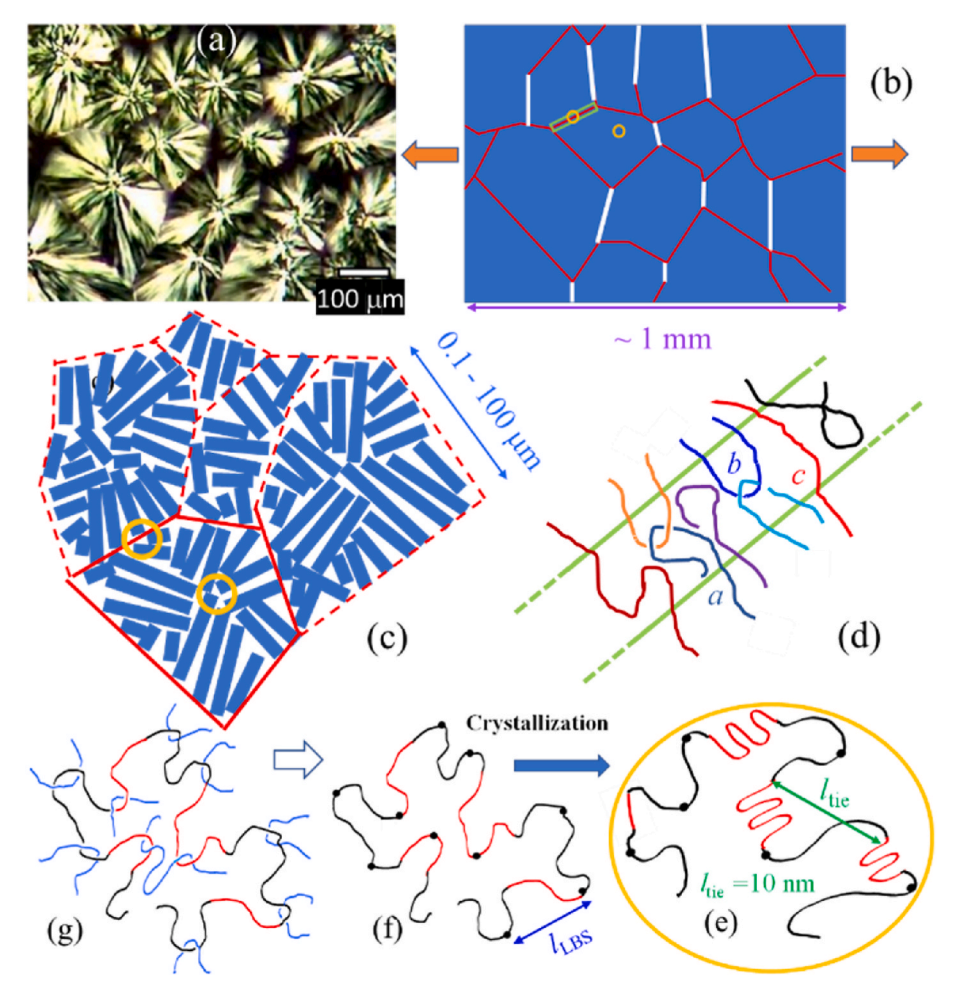


Fig. 1. (a) Typical image of iPP under polarized optical microscope (POM). Typical drawable iPP prepared from melt crystallization have much smaller spherulites (e.g., micron-sized) so that this POM can be regarded as a direct magnification of its morphology. (b) Traces of the spherulitic boundaries based on (a) where the white lines show interstitial regions under extension during "horizontal" drawing, indicated by the arrows. (c) A collection of spherulites that are clusters of lamellae, represented by the thick blue (color online) bars, forming grain boundaries indicated by the thin lines. (d) Illustration of an amorphous region at an interspherulitic boundary, showing chain a as bridging strand, chain b as entangling strand, and chain c as tie strand. We call tie and entangling strands collectively connecting strands. This interspherulitic boundary, e.g., the region circled in (c), is merely amorphous, without lamellae. The cartoon is similar to one in Ref. [13]. (e) For clearer illustration of a test chain, located at the intraspherulitic circle in (c), the crystalline segments are depicted in red (color online), while the amorphous segments are in black, where black dots represent the segments involved in interchain constraints by other chains when traced back through (f) and (g) to the original amorphous chain network in molten state. (f) Depiction of the test chain, characterized by ten dots to represent presence of nine load-bearing strands, comprised of amorphous (black) and to-be-crystallized (red) segments. In comparison, only six dots remain in (e) after crystallization, which is expected to remove some uncrossability constraints. The illustration includes both chain folding and lack of adjacent re-entry, i.e., a straight red strand. The size of 10 nm is speculative. (g) Sketch of a chain network in the molten state, featuring the test chain (in black and red color online) constrained by the surrounding chains due to the interchain uncrossability where the pairs of hairpins may be viewed as the network junctions. (For interpretation of the references to color in this figure legend, the reader is referred to the Web version of this article.)

acting as "rigid fillers". An SCP is a collection of highly rigid space-filling spherulites, with connecting strands between the neighboring spherulites to hold the "composite" structure together. Above $T_{\rm g}$, apart from causing the SCP to appear rigid, lamellae act like crosslinking to immobilize chains, making the SCP behave like a solid.

S.-Q. Wang et al.

Fig. 1(e) depicts a test chain in an SCP. Hereafter we refer to SCPs in terms of chains and strands interchangeably whenever there is no confusion. During crystallization, portions of the chain (i.e., red subchains - color online) join lamellar crystals. Fig. 1(f) shows the conformation of the entire test chain before crystallization: It belongs to a chain network shown in Fig. 1(g). Here the interchain uncrossability establishes an entanglement network so that in the molten state we can envision the test chain to be constrained at ten points, denoted by the ten black dots in Fig. 1(f). In the crystalline state, if the crystallization is fast, this test chain can be expected to participate in both lamellar crystallization and chain networking in amorphous phase. Because crystallization depletes certain uncrossability constraints, fewer pairs of hairpins are present after crystallization so that the CCN is bound to have reduced density of load-bearing strands (LBSs), as shown by the fewer dots (decreasing from ten to six) in Fig. 1(e). We note that the effect of crystallization on entanglement has been suggested before [16-20]. Specifically, MD simulations [19,20] suggested a decrease of entanglement during crystallization. Moreover, Strobl and coworkers [17] also suggested an SCP to be modeled as a network: "The network is set up by the chain entanglements which act like cross-links." In our picture, crystalline domains play a more dominant role as "crosslinkers" to fix the chain network. In passing, we note the recent attempt [21] to quantify chain entanglement in the amorphous phase using ¹H NMR T₂ relaxation measurements.

As depicted in Fig. 2(a), an SCP may be symbolized as a crystallization-fortified chain network, or in short crystalline chain network (CCN) in which there are "permanent" junctions denoted by red dots (color online) due to entrapment of subchains into lamellae and junctions (denoted by the crosses +) due to interchain uncrossability. At high sufficient crystallinity there are enough dots in this 3D CCN, of which Fig. 2(a) is an abstract 2D representation. Here chains converging to the dots are tie chains or entangling strands. Thus, the CCN concept demonstrates the role of connecting strands as linkage between crystals and amorphous regions. In other words, CCN recognizes what it means for a chain to be embedded in both crystalline and amorphous phases and that a test chain in the CCN has both crystalline and amorphous strands. In such a CCN long chains would remain linked to one another even in the absence of any entanglement (topological uncrossability) as shown in Fig. 2(b). Since the isolated dangling strands are not load bearing, the skeleton of Fig. 2(b) is actually Fig. 2(c), showing the effective connectivity. If any one of the six dots in Fig. 2(b) is missing, there is no longer a permanent network when entanglement is also

absent. Fig. 2(b') is an example with four dots as the skeleton of Fig. 2 (a'). If Fig. 2(a') is true on a global scale, the SCP would not be a solid above T_g due to lack of adequate crystallization. This of course is usually not the case for SCPs. With relative fast crystallization there is usually sufficient crystallization for SCPs, and there are usually entanglements trapped between crystals. The case of Fig. 2(a') simply does not arise.

We have used Figs. 1 and 2 to indicate some generic structural hierarchy in SCPs. It is crucial to emphasize that these features change in significant ways, depending on the thermal history leading to the crystalline state. In other words, different structures of the CCN may result, characterized by different levels of crystallinity and disruption of the chain network. Although direct experimental evidence of the structural variations is hard to obtain, various mechanical characteristics of the same SCP, as dramatic as exhibiting brittle versus ductile behavior during large tensile extension, reflect the structural variation. For example, we show in 3.1.2 of Paper 1 (this volume, p. 125878), based on several SCPs, how widely varying mechanical responses are observed depending on sample preparation procedures. Section 8 below will further discuss the effect of crystallization on ductility.

3. Mechanical relation between amorphous regions and crystalline phase: stress whitening

It is instructive to regard an SCP as a structural hybrid, made of agglomerates of lamellae that pile up to form spherulites. In the hierarchical structures depicted in Fig. 1(b)-(g), ranging from strands (ca. 10 nm), lamellae (e.g., $10 \text{ nm} \times 10 \text{ }\mu\text{m}$), and spherulites (e.g., $100 \text{ }\mu\text{m}$) to the macroscopic dimensions (1 mm), amorphous regions reside both inside spherulites and at interspherulitic boundaries. Upon full or saturated crystallization, the amorphous regions can all be expected to be much smaller than the chain coil size characterized by the radius of gyration R_g. Tie strands may be present to connect neighboring lamellae as illustrated in Fig. 3 by the red (color online) lines of chains 2 and 3, along with entangling (green color online) chain 1 with other chains emanating from neighboring lamellae. In a ductile SCP of high molecular weight, entangling chains are numerous due to uncrossability while the bridging strands are dangling strands (cf. chains 4 and 5 in Fig. 3) and therefore statistically negligible. Entangling strands (e.g., chain 1 in Fig. 3) can act like tie strands at fast local strain rates (relative to chain dynamics) or low temperatures, as proposed before [22,23]. Since Keith et al.'s observation [24] of fibrils between crystals that are understood to be bundles of tie strands, tie strand has been a widely used concept [8] in the description of the mechanics of SCPs [22,25-30], with some emphasizing [22] that entangling chains can play the same role as tie strands do. The number of entangling chains in the amorphous phase depends on the crystalline morphology through thermal history and thus depends on the extent to which the chain network is depleted by the

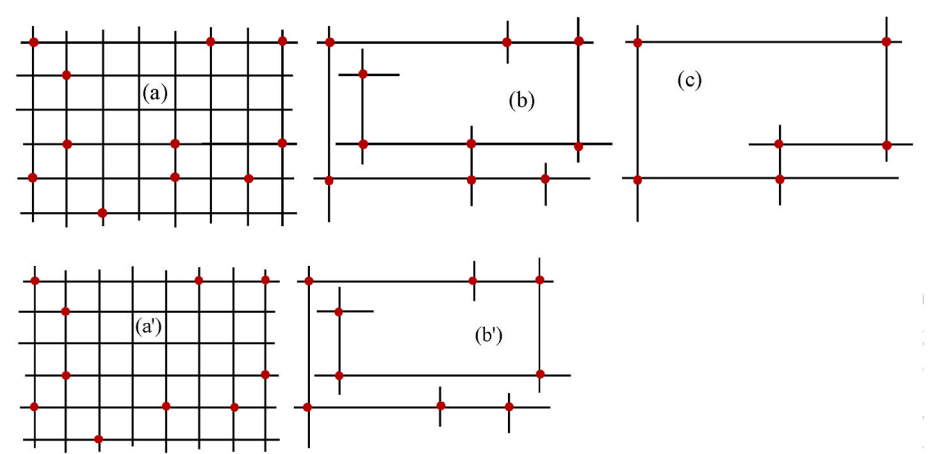


Fig. 2. (a) Abstract 2D representation of CCN, where red (color online) dots denote crystalline domains that embed amorphous chains and crosses + are the network junctions due to interchain uncrossability. (b) At long times, the permanent connectivity is provided by the presence of crystallization, revealing the skeleton of the CCN. (c) The minimal connective structure corresponding to (a). (a') A second scenario with fewer crystalline domains. (b') The structure of (a') at long times, showing it is not a CCN but a linear object. (For interpretation of the references to color in this figure legend, the reader is referred to the Web version of this article.)

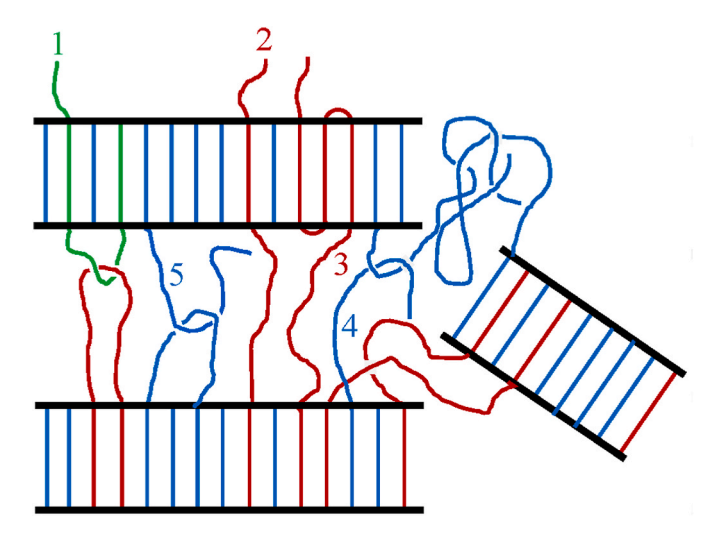


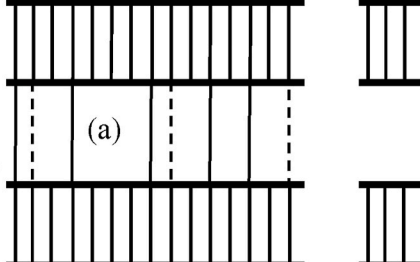
Fig. 3. Structural features at the lamellar level showing chain 2 and chain 3 contribute as tie strands, chain 1 contributes as an entangling strand that can act like a tie strand at high rates, chain 4 entangles with a long bridging strand, and chain 5 bridges with an entangling strand. In the presence of sufficient crystallization, an "interior" strand of a long chain (e.g., chain 1 or chain 2) must either be a tie or entanglement strand. Chains 1, 4 and 5 have been termed entangled chains in MD simulation [23]. In our picture, entangling strands of chains 4 and 5 play little role because there are so few of them.

crystallization. It is noted in passing that the importance of polymer entanglement over the presence of tie strands has been emphasized in a previous study [31] of the tensile deformation of SCPs.

Zooming out, as shown in Fig. 1(c), we contemplate that the lamellae are jammed into clusters (i.e., spherulites) that touch upon one another at the grain boundaries (dashed lines). While small deformation of these spherulites can take place without breakdown of the intraspherulitic lamellae, their large deformation should be associated with either melting and recrystallization to accommodate the volume-conserving shape-change of spherulites or fragmentation of the crystallization phase, resulting in interstitial or intraspherulitic cavitation. In our view, fragmentation [10] and melting [11] are both caused by massive chain pull-out, which is disengagement of a crystalline stem, e.g., moving out of a lamella, whereas crystallographic slip [12,17] might be regarded to involve modest pull-out. Ductile SCPs can either show yielding without stress whitening, as is the case in room-temperature uniaxial drawing of PE and high temperature drawing of PP (cf. 3.1.3 of Paper 1 (this volume, p. 125878)), or exhibit whitening to indicate the occurrence of cavitation, e.g., during room temperature drawing of PP (cf. 3.1.3 of Paper 1 (this volume, p. 125878)). The type I whitening occurs at small strains and is reversible, i.e., disappearing upon unloading. This type I is plausibly associated with cavitation in the amorphous phase due to the lack of transverse contraction of crystalline domains (e.g., spherulites).

Brittle fracture or complete lack of drawability may be regarded as an extreme form of structural failure, involving excessive drawing of interspherulitic regions to failure before intraspherulitic transformation (cf. POM movie in 3.1.7.3 of Paper 1 (this volume, p. 125878)). Fig. 4 depicts the two extremes: (a) sufficient connecting strand density to permit transformation of lamellar phase so that type I whitening might be avoided, as is typically the case of PE; (b) sparse tie strand density so that tie strand pull-out is unable to bring about plastic deformation of the crystalline phase, and separation takes place between the two lamellae, leading to cavitation and potential subsequent macroscopic separation. Depending on thermal history, a given SCP may be described by either Fig. 4(a) or Fig. 4(b), so that it can be either ductile or brittle as shown in 3.1.2 in Paper 1 (this volume, p. 125878). Fig. 4(a) will also later be used to account for different temperature and rate dependencies of common SCPs such as PP.

Besides extensive experimental investigations (cf. 3.1.3 of Paper 1



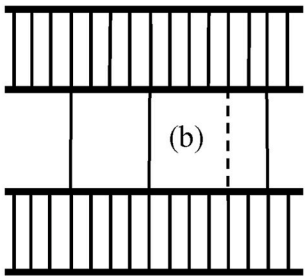


Fig. 4. Sketch to show (a) significant connecting (tie and entangling) strand density between two neighboring crystalline domains (lamellae or spherulites) and (b) sparse connecting strand density. Here tie strands are designated by the solid lines and entangling strands that act like tie strands (at lower temperatures or higher rates) are represented by dashed lines.

(this volume, p. 125878)), MD simulations [23,32–35] attempted to describe cavitation in the amorphous layer between two parallel lamellae. When there are enough connecting strands between the two lamellae to enable plastic deformation of the lamellae, cavitation may be avoided. Consistent with whitening behavior in PP (cf. 3.1.3 of Paper 1 (this volume, p. 125878)), cavitation is more difficult to avoid at faster drawing rates – at lower rate the crystalline phase has time to undergo sufficient transverse contraction upon melting, permitting the amorphous region to stretch with volume conservation [23].

The cohesive strength of an SCP may depend on how grain boundaries respond during external deformation. Thus, certain interspherulitic regions (indicated by white lines in Fig. 1(b)) should be the key object for investigation. POM observations reported in 3.1.7 of Paper 1 (this volume, p. 125878) support such insights. When an SCP is drawn horizontally as shown Fig. 1(b), the interspherulitic regions depicted by near-vertical white lines are loaded. Above T_g , these amorphous regions are far more compliant than rigid spherulites. Consequently, they undergo excessive straining, far greater than the imposed nominal strain. In other words, rigid spherulites greatly amplify the strain experienced by the interstitial regions because, as shown in Fig. 5(a), the width δ of

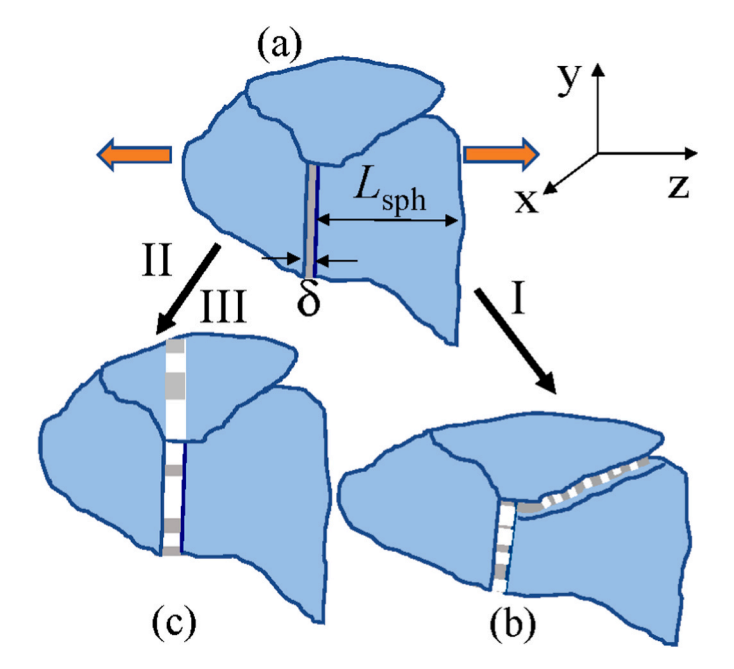


Fig. 5. Structural failure of different types, interspherulitic and intraspherulitic, in tensile drawing of SCPs, from the undeformed state (a) to (b) that may be regarded as an illustration of type I whitening, and from (a) to (c), corresponding to type II or III whitening. Brittle fracture in glassy SCPs may also take such paths.

the interspherulitic boundary is typically much smaller than the average spherulitic size $L_{\rm sph}$. Thus, while the crystalline phase undergoes little drawing, i.e., when an applied nominal strain $\varepsilon \ll 1$, the interspherulitic layer undergoes an amplified extension that can be estimated to be

$$\lambda_{\text{intersph}} \approx 1 + \varepsilon \left(L_{\text{sph}} / \delta\right)$$
 (1)

Because the strain amplification factor $L_{sph}/\delta\gg 1$, a high degree of drawing can take place between certain spherulites, potentially leading to cavitation as illustrated in Fig. 5(b). Here and in Fig. 5(c) we envision the possibility that multiple cavities can arise in either interstitial or intraspherulitic manner. The POM observations in 3.1.7 in Paper 1 (this volume, p. 125878) demonstrate this strain amplification effect.

The strain amplification arising from the elastic disparity is the cause for the various types of whitening. Interspherulitic cavitation occurs when spherulites are yet to or unable to contract transversely to the drawing direction (Z axis) as shown in Fig. 5 from (a)-(b). Such cavitation might be largely reversible, i.e., the corresponding whitening diminishing upon unloading. According to observations of PP presented in 3.1.3 of Paper 1 (this volume, p. 125878), the severe type II is accompanied by volume non-conservation while type III whitening has been defined in 3.1.3 of Paper 1 (this volume, p. 125878) as a milder form in post-yield drawing. It is plausible that type II also involves significant intraspherulitic cavitation from Fig. 5(a)-5(c), showing fragmentation [10] of spherulites. In contrast, there may be adequate recrystallization after melting [11] of the crystalline phase to avoid crystal fragmentation in type III whitening that is observed at slow rates. Finally, at high strains and elevated temperatures [36], e.g., at 90 $^{\circ}\text{C}\text{,}$ well after completion of necking, severe whitening can take place, as shown in Figs. 7 and 9 of Paper 1 (this volume, p. 125878). This type IV whitening plausibly stems from the rising chain tension that overcomes the cohesion provided by the crystalline phase, i.e., involving chain disengagement from the CCN due to pull-out from the crystalline phase. The chain retraction along the drawing direction upon the force imbalance nucleates cavitation. As the significant geometric condensation of the CCN hinders transverse contraction, the cavities only further grow by elongating. At such high strains, the structure of CCN is also especially weak perpendicular to the drawing direction, making it also easy for shear failure to take place, leading to splitting. Section 3.1.3 in Paper 1 (this volume, p. 125878) showed the conditions for each type of whitening.

The detail about how why and how cavitation forms has been reported by Galeski and coworkers [37]. For example, they suggested [38] cavities originate from free volume pores. They showed [39] that cavitation usually emerges upon yielding not before yielding. Depending on how yielding is defined, Fig. 5(a) in Paper 1 (this volume, p. 125878) shows discernible type I whitening before the stress peak. It was also pointed out in the literature [40] that "cavitation occurs in polymers with crystals of higher plastic resistance", which is consistent with our understanding that lack of crystal deformation leads to type I cavitation. To reiterate, when crystals are largely intact amorphous regions between the crystals extend without transverse contraction, leading to negative pressure due to the volume expansion so that cavitation become inevitable. Intraspherulitic or intra-crystal cavities are a different type, belonging to type II and III, as illustrated in Fig. 5 and observed in POM 3 in Paper 1 (this volume, p. 125878), explicitly reflecting structural failure of the crystalline phase.

At the end of this subsection, a few remarks are in order. First, while the mechanical function of lamellae has been recognized as providing crosslinks, it is imperative to acknowledge the structural role of the LBSs that include chains 1, 2 and 3 as connecting (tie and entangling) strands, and 4 and 5 as bridging strands (cf. Fig. 3). These LBSs between crystalline domains are the "invisible" hands through which the crystalline phase may undergo deformation via chain pull-out. Conversely, if large deformation of spherulites is not possible due to lack of chain pull-out, massive interspherulitic straining occurs, leading to interstitial

cracking. POM observations have been made to reveal the interstitial tensile failure in 3.1.7 of Paper 1 (this volume, p. 125878). At the chain level, the eventual macroscopic separation during drawing above T_g involves the localized breakdown of the CCN via pull-out of connecting strands from the crystalline phase. In passing, we note that chain pull-out does not necessarily imply loss of connecting strands. For example, one stem can pull out from the upper lamella, e.g., that of chain 3 in Fig. 3 while the other two stems remain, i.e., chain 3 is still embedded in the lamella if the lamella adjusts to fill the molecular hole left by the pull-out. Here molecular models are desired to describe how the lamella responds to the pull-out event. It is also desirable to separate the effect of crystallization on entanglement from that on crystalline morphology. Such a topic is well beyond the scope of the present work.

4. High Young's modulus of rubbery SCPs and threshold pull-out force near $T_{\rm m}\,$

Crystallization not only serves the function of crosslinking for rubbery SCPs but also allows SCPs to be highly rigid, with E reaching the level of 1 GPa, comparable to that of glassy polymers. Reading from Fig. 2(d) in 3.1.1 of Paper 1 (this volume, p. 125878), we see that E of rc-PP is temperature dependent and of high magnitude, e.g., ca. 700 MPa at room temperature and 170 MPa at 90 °C in contrast to its melt plateau (shear) modulus G on the order of ca. 1 MPa in the absence of crystallization. This high rigidity reveals that the crystalline phase has a high modulus. If lamellae are taken to show Young's moduli Elam(||) and $E_{lam}(\perp)$, defined with respect to the lamellar orientation, and the amorphous phase has modulus $E_a \sim G$, the Young's modulus of a typical spherulite, E_{sph} , may be on the order of $E_{lam(||)}$ or $E_{lam}(\perp)$, since spherulites are made of lamellae in a jammed state (cf. Fig. 1(c)). Then, E of an SCP is lower than E_{sph} as the SCP is a composite made of spherulites impinging one another at the interstitial rubbery boundaries. There are two extremes according to the Voigt and Reuss averaging schemes respectively [1]. We either have

$$E_{Voigt} = \alpha_{sph} E_{sph} + \left(1 - \alpha_{sph}\right) E_a \;\cong\; \alpha_{sph} E_{sph} \tag{2} \label{eq:2}$$

or

$$E_{Reuss} = E_{sph}E_a/[\alpha_{sph}E_a + E_{sph}(1-\alpha_{sph})] \cong E_{sph}/\alpha_{sph}, \tag{3}$$

where α_{sh} is the volume fraction occupied by spherulites, and the second expression in Eq. (3) following if the two terms in the square brackets are comparable in magnitude. Since $\alpha_{sph} \sim 1$, both Eqs. (2) and (3) show E of typical SCPs with high crystallinity to be given by E_{sph} . When the crystalline phase is no longer space filling, the above analysis is invalid. Below we examine a case of $E_{lam(||)} \sim E_{sph}$.

We have previously shown [41] that shear melt plateau modulus may be regarded as a product of an areal density ψ_{ent} of entanglement strands and characteristic entropic force f_{ent} associated with such strands, i.e., $G_{N}^{0}=\psi_{ent}f_{ent}.$ Analogously we write Young's modulus E_{lam} of a lamella in terms of an areal density ϕ of covalent bonds and a characteristic force f_{lam}

$$E(lam(\parallel)) = \varphi f_{lam} \tag{4}$$

where φ is the reciprocal of the bond cross-sectional area s that can be characterized in terms of the Kuhn length $l_{\rm K}$ and packing length p as [41].

$$\varphi = 1/s, s = pl_{\mathbf{K}}.\tag{5}$$

Here we assume that stems in a lamella are packed to the maximal density of one stem per area of s. We may take f_{lam} as the pull-out force required for a tie strand to disengage from a lamella and we can expect $f_{lam}(T)$ to become vanishingly small as the temperature approaches melting point T_m . In other words, Eq. (4) allows us to describe $E(T) \sim E_{lam(||)}(T)$ and yield stress $\sigma_v \sim \sigma_{cv}(T)$ with the same temperature

dependence (cf. Fig. 2(d) in Paper 1 (this volume, p. 125878)).

According to recent direct atomic force microscopy (AFM) measurements [42-44], the pull-out force has some weak dependence on lamellar thickness and is on the order of a tenth of a nano-Newton. Given a typical $p \sim 0.2$ nm and $l_K \sim 1$ nm from the literature [45,46], with f_{lam} ~ 0.1 nN, we have $E_{lam(||)}$ to be on the order of 0.5 GPa well below T_m , matching E of typical SCPs. If the temperature dependence of E(T) may be taken as reflecting that of $f_{lam}(T)$ then according to Eq. (4) f_{lam} would decrease by a factor of four for PP from room temperature to 90 °C (cf. Fig. 10 in Paper 1 (this volume, p. 125878)). We could also estimate f_{lam} from theoretical considerations, e.g., relating it to the free energy difference between an embedded strand in a lamella and the same strand in amorphous state. However, such an argument does not lead to a satisfactory prescription for the temperature dependence of $f_{lam}(T) \sim E(T)$, which appears to be a rather strong function of T according to Fig. 2(d) of Paper 1 (this volume, p. 125878) upon approaching T_m. While temperature dependence of modulus of glassy polymers has been described by an activated barrier hopping theory of deeply supercooled melts [47], the temperature dependence of E(T) for SCPs may be more challenging to formulate.

5. Yielding: role of connecting strands in plastic transformation of crystalline phase

All viscoelastic materials (in either liquid or solid state) undergo yielding at large deformation. In the solid state, viscoelastic materials including SCPs may be regarded as yield-stress materials. Creep tests indeed reveal the cohesive strength of SCPs, as shown in 3.1.1 of Paper 1 (this volume, p. 125878). In absence of tie strands, SCPs would be like a "pile of wet sand", i.e., having negligible cohesion and unable to withstand large deformation. Because of dense tie strands, SCPs of high molecular weight are rigid and tough.

Yielding or breaking in SCPs depend explicitly on how connecting strands build the bridges between spherulites and among lamellae within spherulites. When crystallization achieves the effect of "crosslinking" all chains into a single structurally connected entity, of which Fig. 2 is an abstract representation of an infinitesimal region, tie strand pull-out is inevitable at high strains of displacement-controlled continuous drawing, leading to crystal fragmentation and melting. Volume-conserving or near-volume-conserving tensile extension of SCPs beyond yielding can prevail when pull-out of connecting strands induces lateral contraction of spherulites through melting and recrystallization to permit plastic or partially plastic deformation of the crystalline phase. In an idealized case of drawing between two parallel lamellae, the united-atom model for PE has been used [23,35] to show how lamellae can undergo lateral contraction to prevent type I whitening, i.e., cavitation in the amorphous region, e.g., at interspherulitic boundaries.

Ductile SCPs show yield stresses typically on the level of tens of MPa. For example, PP shows yielding in the range of $\sigma_y=20$ –40 MPa according to both creep and displacement-controlled drawing (cf. 3.1.1 and 3.1.2 of Paper 1 (this volume, p. 125878)). If we assign an effective areal density of LBS ψ_{LBS} , tension in LBS f_y at the yield point, leading to chain pull-out, may be estimated as $f_y=\sigma_y/\psi_{LBS}=(\sigma_y/\phi)(\phi/\psi_{LBS})>\sigma_y/\phi=6$ pN, with ϕ given in Eq. (5) and taking $\sigma_y=30$ MPa, p=0.2 nm and $l_K=1$ nm. We note that 6 pN is comparable to the limiting magnitude of the entropic force $f_0=k_BT/l_K\sim 4$ pN at T=300 K. Thus, f_y has 6 pN as its lower bound and is perhaps also the lower bound of f_{lam} introduced in Section 4.

The cartoon in Fig. 1(c) may be taken as an approximate depiction of typical spherulitic morphology in SCPs, based on the available knowledge that spherulites are a collection of lamellae. The crystalline plasticity implies a breakdown of this jammed state of lamellae. According to Fig. 1(c), no appreciable orientation of lamellae can take place without lamellar structural breakup in the form of either melting followed by recrystallization or fragmentation. Connecting strands are the drivers for this transformation. Specifically, when spherulites impinge

on one another, i.e., are space filling, crystallographic slip can hardly be the only form of structural response at the yield point. Past studies [22, 48–50] have extensively focused on ductile drawing of SCPs, where yielding has been explained to take place through either fragmentation [10,17], crystal melting [11,51,52] or crystallographic slip [12,17].

Here we emphasize that sufficient areal density ψ_{tie} of tie strands emanating from spherulites and lamellae inside spherulites is only the necessary but not the sufficient condition for yielding. Successful yielding requires a subtle balance: In ductile drawing, as the lamellar transformation continues, either enough lamellar crystals survive or recrystallization occurs after the mechanical melting so that enough crystals are present to serve as "crosslinkers". If considerable lamellar melting occurs but the recrystallization is too slow to re-entrap enough tie strands to avoid the situation depicted by Fig. 2(b'), the drawing will terminate due to the structural failure of CCN. In other words, for an SCP to yield and avoid structural breakdown, crystallization should have retained an adequate chain network. On the other hand, there must be enough pull-out events involving connecting strands to permit crystal transformation: In the absence of sufficient pull-outs, transverse contraction could not take place, and the strain amplification would continue to grow between neighboring spherulites until macroscopic separation. In short, yielding of SCPs upon large deformation requires the CCN to be sufficiently robust, capable of structural adjustment in post yield to retain global structural integrity.

Although the present study aims to discuss lack of drawability, we can make a comment on the competing ideas concerning the structural change that accompanies yielding in an SCP. First, according to Strobl and coworkers [17,53], crystallographic slip precedes crystal fragmentation at the beginning of yielding, followed by fragmentation and chain disentanglement. Can this structural slip occur without pull-out of connecting strands? In other words, what do connecting strands do to cause slip and fragmentation? If these Strobl processes are to involve chain pull-out, how are they different from melting? We think that the slip should be regarded as a form of melting. Ductile drawing of rc-PP at room temperature clearly shows a reduction in crystallinity in Fig. 10(c) in Paper 1 (this volume, p. 125878). The effect of drawing on the crystalline phase is less at 90 °C. These observations are consistent with in situ x-ray study [22] of Zuo et al. Similar features are observed in late-stage tensile drawing of LLDPE in Fig. 12(d) in Paper 1 (this volume, p. 125878). As evidence of recrystallization, drawing of iPP led to increase crystallinity as shown in Fig. 12(e) through 12(g) in Paper 1 (this volume, p. 125878).

While data in Figs. 10 and 12 in Paper 1 (this volume, p. 125878) involve strong necking in the late stage of postyield drawing, it is instructive to capture the structural changes at the beginning of yielding. Four discrete drawings of rc-PP were made at room temperature to produce different levels of postyielding, i.e., past the yield point corresponding to the peak tensile force, as shown in Fig. 6(a)-(b). 1D WAXD profiles in Fig. 6(c) show that there are discernible changes at B that involve a local draw ratio of ca. 1.2 and hardly show any noticeable necking. Specifically, at point B there is a measurable loss of crystallinity, plausibly due to a small amount of stem pull-out. Until there is reliable quantitative modeling to correlate such changes in the characteristics peaks with the crystal plasticity induced by pull-out, it is sufficient to acknowledge these changes without labeling them as crystallographic slip, melting, or fragmentation. On the other hand, there is appreciable reduction in crystallinity at C, which is evidence for melting. Throughout our two papers, melting means disintegration of certain crystals due to stem pull-out, which need not take place at temperatures above the melting temperature T_m (cf. Section 12 below).

6. Temperature effects (above Tg) on drawability

As shown in Paper 1 (this volume, p. 125878), drawability varies from one SCP to another. For a given rubbery SCP, ductility and ability to yield depend on thermal history, temperature and drawing rate. Is

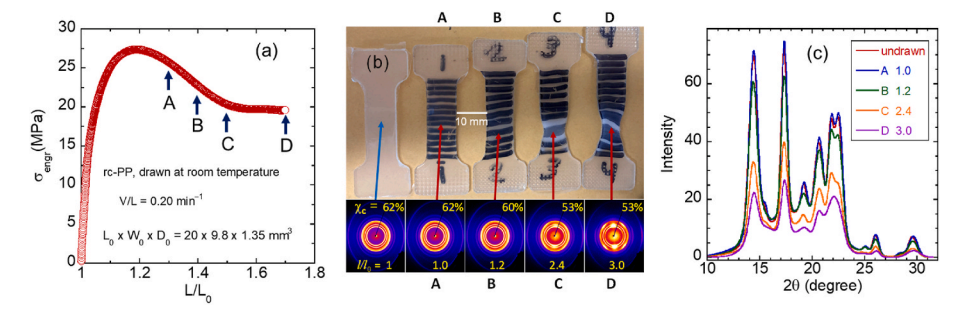


Fig. 6. (a) Stress-strain curve of rc-PP dogbones (of type **2**) drawn at room temperature at $V/L = 0.20 \, \mathrm{min}^{-1}$ to varying nominal draw ratios $L/L_0 = 1.3$ (A), 1.4 (B), 1.5 (C), and 1.7 (D). (b) Photograph of the four specimens after drawing and unloading, showing the progression of necking. A percent of length (elastic) retraction is observed upon unloading, as expected. *Ex situ* WAXD were taken at the positions indicated in the photograph. (c) 1D WAXD from (b) showing discernible change at point B and gradual loss of crystallinity with increasing local strain.

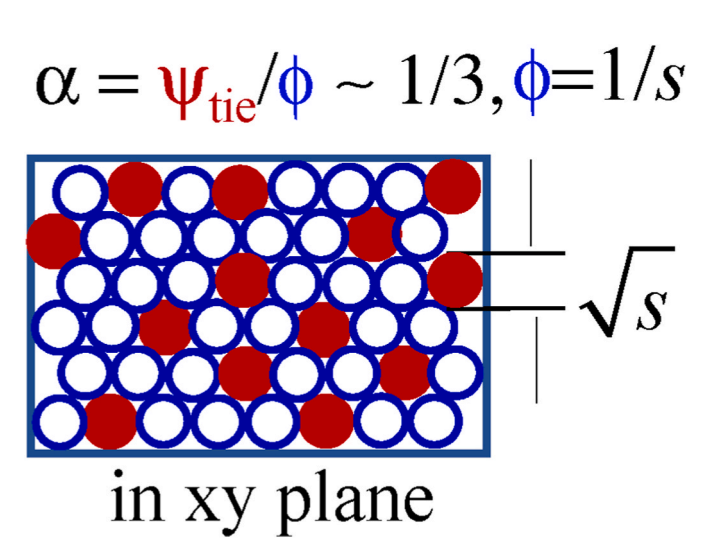


Fig. 7. Illustrative view of a lamella showing ca. 1/3 of strands sticking out the lamellar plane to form tie strands.

there a common explanation for lack of ductility and drawability? What would be the failure mechanism? Spherulite is an important structural entity, and its deformability is necessary for SCPs to undergo large deformation and acquire drawability. Strength of interspherulitic layers determines whether spherulites can sufficiently deform so that yielding of the crystalline phase occurs to avoid fracture. While various cartoons [15,37,54] have speculated about how a spherulite deforms in extension, no quantification exists in the literature for why large spherulitic deformation fails to take place for a given SCP under a given condition.

Stable structural transformation and large deformation of rigid spherulites occur through meltdown of spherulites without breakdown of the CCN. Sufficient chain pull-out is a necessary condition for crystalline transformation. When pull-out is sparse at interspherulitic boundaries due to a lack of tie and entangling chains, rigid spherulites are unable to achieve structural adjustment. Amplified straining inevitably occurs in interstitial layers leading to interspherulitic cavitation and subsequent fracture. More pull-out may also result in crystalline fragmentation that could take place in the form of intraspherulitic cavitation (cf. Fig. 5). Thus, depending on the areal density of connecting strands at interstitial boundaries, fracture can be either purely interspherulitic (if the connecting chain density is particularly low) or involves a mixture of intraspherulitic and interspherulitic separations.

The effect of temperature on ductility has been demonstrated for several SCPs in 3.1.4 of Paper 1 (this volume, p. 125878). HDPE, iPP and rc-PP all turn from brittle-like response to ductile drawing when the experimental temperature is elevated above room temperature. Given the preceding discussion about non-drawability, the observed brittle-like responses of these three SCPs at room temperature imply insufficient pull-outs and relatively low areal density of connecting strands in these SCPs. At elevated temperature, it is clear that the amount of pull-

out becomes sufficient to induce melting of the crystalline phase (e.g., spherulites), which can be accompanied by a variety of transformation including crystallographic slip [17,54]. With rising temperature, the alpha relaxation process in the crystalline phase has increased appreciably [55,56], enabling pull-out to induce sufficient meltdown of the crystalline phase. We note that rc-PP shows brittle-like response at room temperature because a relatively high rate was applied. At such a high rate, the number of pull-out events is not sufficiently high to induce melting at room temperature where alpha relaxation time in the lamellae is long, relative to its value at elevated temperatures. We separately know that rc-PP shows ductile response at lower drawing rates. Thus, rate has an effect that is as understandable as the temperature effect. More discussion on the rate effect is deferred to the following section. In conclusion, our preceding explanation is actually consistent with recent computer simulation results [23] that reveal either amorphous cavitation at high rates or crystalline transformation at low rates or faster chain dynamics to save the SCP from cavitation.

6.1. Implication of temperature dependence of yield stress

Well above Tg, the time-temperature superposition principle works well even for nonlinear rheology of entangled melts [57]. Thus, as far as the mechanical response is concerned, one might expect the effect of lowering temperature to be equivalent to applying a higher drawing rate. According to the preceding discussion, at a lower temperature, a higher stress would emerge as the system enlists entangling chains to join the resistance to drawing. Data in 3.1.4 of Paper 1 (this volume, p. 125878) show that the yield stress in PP changes by a factor of four from 90 °C to room temperature. This change is perhaps too large to be accounted for by the effect of entangling chains, i.e., by claiming that the areal density of connecting strands at interspherulitic boundaries, $\psi_{intersph}(T)$, quadruples upon the temperature change. Plausibly, this temperature dependence implies that the crystalline phase is much less resistant to plastic deformation at a higher temperature, and the chain pull-out force $f_{lam}(T)$ decreases with increasing temperature. Consistent with this speculation, we note that Young's modulus changes by a similar level, which has been explained in terms of the temperature dependence of f_{lam} in Section 4.

Furthermore, creep data in 3.1.1 in Paper 1 (this volume, p. 125878) indeed indicate that the cohesive strength weakens with rising temperature: at a higher temperature the threshold tensile stress required to initiate plastic deformation is lower by the same amount as Young's modulus. Currently, no first principles theory is available to describe the relationship between $f_{\rm lam}$ and T. While such a relation would be a first step in the description of the stress response of SCPs, it is insufficient to use the information to predict when SCPs loses drawability. Upon drawing, chain pull-out will take place whether it meets higher or lower resistance. The challenging task is to describe how drawability of SCPs depends on temperature.

6.2. Opposite effects

It is remarkable that temperature can have opposite effects on

ductility for different SCPs, and even for the same SCP, as documented in 3.1.4 of Paper 1 (this volume, p. 125878). We proceed with a simple explanation about crystalline meltdown, relating the amount of chain pull-out events to the areal density of connecting strands and hypothesizing that with increasing temperature, plastic deformation of the crystalline phase requires fewer pull-outs. With marginally low density of connecting strands, rise of temperature can be sufficient for an SCP to turn from brittle to ductile. This is apparently the case of the polyolefins, e.g., HDPE, iPP and rc-PP (cf. Figs. 10 and 12 of Paper 1 (this volume, p. 125878)). However, when the number of connecting (tie and entangling) strands are too sparse to induce melting, raising temperature may not help. Fig. 13 in Section 3.1.4.2 of Paper 1 (this volume, p. 125878) reveals such counter-intuitive temperature dependence of PHA. We suggest that the loss of ductility in PHA with rising temperature occurs when, due to the faster chain dynamics, fewer entangling chains are load-bearing and, thus, fewer contribute to pull-out. Without sufficient crystalline transformation, interstitial layers experience excessive extension, leading to interspherulitic breakup.

The ductility of ccPLLA also shows non-monotonic temperature dependence (cf. Fig. 8 of Paper 1 (this volume, p. 125878)). Just above T_g , raising temperature promotes ductility, implying crystalline transformation is more feasible with increasing temperature. However, with further rise, from 100 to 130 °C, ccPLLA becomes less ductile/drawable, implying fewer entangling chains can be enlisted to undergo pull-out; sufficient pull-outs are necessary for plastic deformation of the

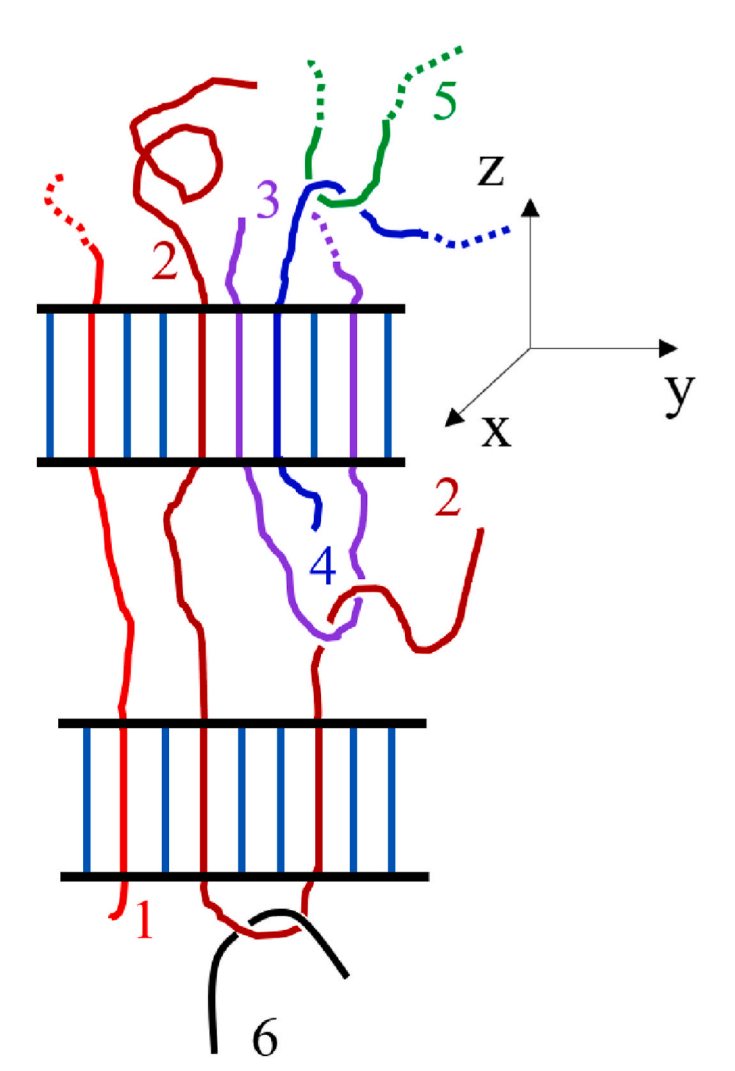


Fig. 8. Structural change through extensive pull-out from lamellae, involving chains 2 through 4.

crystalline phase.

6.3. Cavitation in PP

Pre-yield type I whitening plausibly occurs for lack of sufficient transverse contraction of spherulites, with cavitation located in interstitial regions, as speculatively illustrated in Fig. 5(b). They can disappear upon unloading to permit elastic recoil. Type II likely also involves the intraspherulitic cavitation, depicted in Fig. 5(c). The more severe type II is replaced by type III when the drawing rate is significantly lowered, as shown in 3.1.3 of Paper 1 (this volume, p. 125878). This rate dependence offers valuable insights into the temperature effect on whitening. Specifically, as shown in Paper 1 (this volume, p. 125878), PP exhibits appreciable whitening at room temperature but indiscernible whitening at higher temperatures, e.g., at T = 90 °C. To the leading order, perhaps raising temperature has the same effect as lowering the drawing rate. On the other hand, at higher temperatures, because of higher segmental mobility the crystalline phase has enough time to make adequate structural repair, e.g., to "fill the molecular holes" in lamellae produced by chain pull-outs. Thus, at higher temperatures chain pull-out is more likely to follow melting with recrystallization instead of fragmentation. Consequently, type III whitening may avoid irrecoverable intraspherulitic cavitation. Since type IV typically occurs at high strain deep in the post-yield regime, it plausibly involves localized disintegration of the chain network through pull-out, with little chain scission. This insight arises from the argument [58] that little chain scission is required for the yielding of a glassy polymer.

Below T_o, crazing in non-crystalline polymers resembles cavitation in glassy SCPs. While crazing may be bypassed in glassy amorphous polymers such as PMMA, it is hard to avoid whitening in glassy SCPs because SCPs are naturally structurally inhomogeneous, prone to strain localization. Moreover, below Tg the crystalline phase can hardly undergo plastic deformation, exerting constraint on the deformation of the amorphous phase, under which cavitation would readily appear. We cannot rule out that crazing in amorphous regions would not lead to intraspherulitic cavitation as shown in (a) \rightarrow (c) in Fig. 5, leading to intraspherulitic breakup on its way to macroscopic separation. For spherulites to transform, i.e., to undergo large deformation, the lamellae in the spherulites must break up to permit sufficient transverse contraction through conversion of crystalline chains into amorphous ones without breakdown of the CCN. Since crystallization necessarily weakens the chain network by removing interchain uncrossability constraint, SCPs can hardly be ductile below Tg. For example, PP is brittle below T_g (cf. Fig. 10 in Paper 1 (this volume, p. 125878)). Further discussion is deferred to Section 9.

7. Rate dependence: temperature-rate equivalence

Above T_{σ} and in absence of crystallization, linear-chain melts of high molecular weight form transient entanglement networks. Large deformation of such melts belongs to the topic of nonlinear polymer rheology. Due to the interchain uncrossability an entanglement network can homogenously stretch to high strains (e.g., with stretching ratio λ well exceeding three) before some form of tensile strain localization takes place [41]. While the tensile stress level increases with the applied Hencky rate $\dot{\epsilon}$, its magnitude is determined by the melt plateau modulus G_{pl}, on the order of 1 MPa. An eventual macroscopic separation of a specimen into two pieces has been suggested to involve spatially-localized disentanglement due to the molecular force imbalance in the form of mutual chain sliding at junctions [41]. There is also melt rupture at higher rates involving strain hardening and chain scission [59-61]. In SCPs, the chain network is permanent due to crystallization. Unlike the familiar entanglement network in the molten state, the CCN commonly exhibits a stress level much higher than G_{pl} due to the rigidity of space-filling lamellar crystals, acting like rigid fillers.

Equivalent to lowering the temperature, at a higher rate where chain

pull-out occurs on shorter time scales, there may not be sufficient crystalline chain mobility for lamellae to melt down without massive pull-out. In other words, an SCP can lose drawability at a higher rate, as is the case for rc-PP (cf. Fig. 14(a) in Paper 1 (this volume, p. 125878)). In general, a higher stress emerges at a higher drawing rate. This may be understood as follows: with increased drawing rate, more entangling chains are load-bearing, resulting in more mechanical resistance. In general, the areal density $\psi_{intersph}(\dot{\epsilon}~\tau(T))$ of connecting strands across the interspherulitic boundary is a variable, dependent on Weissenberg number $\dot{\epsilon}~\tau(T)$, where $\dot{\epsilon}$ is the amplified local Hencky rate in interspherulitic and inter-lamellar layers (cf. Figs. 1 and 3) and $\tau(T)$ is a temperature-dependent characteristic time for relaxation and disengagement of entangling chains. Thus, at a higher draw rate, more entangling chains can undergo elastic stretching.

As is the case concerning the anomalous temperature dependence discussed in the preceding Section 6.2, the rate effect can also reverse: For cPLLA above Tg, higher drawing rate is shown to produce a more ductile response, as shown in Fig. 8 in Section 3.1.3 of Paper 1 (this volume, p. 125878). This extraordinary rate effect may involve the same physics that explains the anomalous temperature effect in PHA (cf. 3.1.4.3 of Paper 1 (this volume, p. 125878)). Enlisting more entangling chains at higher rates increases pull-out events and enhances the transformation of the crystalline phase to promote drawability. In other words, higher rates engage more entangled chains to participate in crystalline transformation. In general, the temperature change brings about more complicated effects, e.g., affecting chain dynamics, the cohesive strength of the crystalline phase as well as the driving force for recrystallization. This complication is reflected in Fig. 8 of Paper 1 (this volume, p. 125878), showing that the drawability has a non-monotonic trend as the temperature changes from 71 to 130 °C.

In passing, we note that the temperature dependence of $\tau(T)$ is not mechanically accessible from the stress relaxation experiments (cf. 3.1.6 of Paper 1 (this volume, p. 125878)) although dielectric measurements do confirm that the segmental chain dynamics in iPP show substantial temperature dependence [62–64]. From experiment, Hu and Schmidt-Rohr [55] as well as Mano [56] show that the diffusion of PE strands through the crystalline region follows an Arrhenius dependency with temperature, with increased mobility at higher temperatures.

8. Lack of drawability

A deeper understanding of yielding and ductility in SCPs needs to explain when and why an SCP loses drawability in terms of both internal variables such as degree of crystallinity [9] and molecular weight [6] as well external conditions such as temperature and drawing rate [65], as discussed in Sections 6 and 7. In all cases, lack of drawability can be traced back to low areal density of connecting strands and corresponding low level of pull-out, insufficient to induce meltdown of the crystalline phase. Conversely, ductile drawing of SCPs can occur when plastic deformation of the crystalline phase is made possible through sufficient pull-out of LBSs. It is instructive to explore structural failure in terms of hierarchical structures, e.g., recognizing spherulites as entities of considerable significance, which has been emphasized by the *in situ* POM observations in 3.1.7 of Paper 1 (this volume, p. 125878).

8.1. Interspherulitic breakup

In absence of crystallization, in mechanical terms, the structure of the chain network due to interchain uncrossability may be characterized [4] in terms of an areal density ψ_{LBS} of effective LBSs of size l_{LBS} , as shown in Fig. 1(f), whose explicit form is

$$\Psi = 1/pl_{LBS} \sim 1/pl_{K}. \tag{6}$$

It follows from a previous study [4] of glassy polymers that an LBS forms between two pairs of hairpins, and the minimal strand length l_c

between them is proportional to l_K . In a crystalline state, the structural integrity and deformability of spherulites depend on the areal density of LBSs in the CCN. Here we envision an areal density ψ_{tie} of tie strands embedded in intraspherulitic lamellae as well as $\psi_{intersph}$ of connecting strands at interspherulitic boundaries. On the average, ψ_{tie} and $\psi_{intersph}$ are both smaller than ψ_{LBS} because of the depletion of junctions by crystallization. Fig. 1(e)–(f) shows three tie strands in the test chain that had ten LBSs before crystallization. Yielding in glassy polymers occurs when sufficient molecular activation has been produced due to the displacing chain network [4], and post-yield plastic deformation may involve chain pullout as a mechanism to enable deformation of the chain network.

Like an LBS in glassy polymers, in SCPs we can define a tie strand to have an average length of N_{tie} so that there are on the average Z_{tie} tie strands per chain, $Z_{tie}=N/N_{tie},$ where chain length N is expressed in the unit of the number of Kuhn segments per chain. Then $l_{tie}=\left(N_{tie}\right)^{1/2}l_{K}$ represents the average coil size of a tie strand, bridging between two adjacent lamellae, as shown in Fig. 1(e), It is a formidable task to correlate the crystalline morphology with $N_{tie}.$ The areal density ψ_{tie} in the CCN depends on $l_{tie}.$ Specifically, in terms of the bond areal density ϕ in Eq. (3), ψ_{tie} may be expressed as

$$\psi_{\text{tie}} = 1/pl_{\text{tie}} = \alpha \varphi, \text{ with } \alpha = \psi_{\text{tie}}/\varphi = l_{\text{K}}/l_{\text{tie}} = (N_{\text{tie}})^{-1/2}$$
(7)

where α represents the fraction of stems in a lamella that stick out and reach to a neighboring lamella to be counted as a tie strand. Eq. (7) follows from the assumption that the tie strand is a Gaussian coil, which is not a poor approximation according to the literature - the coil size in the molten state is essentially unchanged upon lamellarization [66]. Fig. 7 shows a head-on view of such a lamella with $\alpha \sim 1/3$ whose normal is along the Z axis (cf. Fig. 8). A robust CCN is one with maximum Ztie or shortest l_{tie} or largest α . In terms of Fig. 7 and Eq. (7), the structure of CCN is loosely characterized by α . For example, given $\alpha = 1/3$ in Fig. 7, which appears to be a limit of very high tie strand density, an average tie strand is made of $N_{tie} = 1/\alpha^2 = 9$ Kuhn segments. Currently, the relation between the crystalline morphology and α is unknown. Also unknown is how different morphologies result from different paths of crystallization, determined by parameters such as thermal history, the state of chain entanglement and molecular weight (MW) in the simple case of linear Gaussian chains. High molecular weight (i.e., high Z_{tie}) only minimizes the number of dangling strands and is not a sufficient condition for ductility in SCPs. Conversely, a robust CCN is characterized by a sufficiently small N_{tie} since the basic feature of CCN is given by the tie stem fraction $\alpha = (N_{tie})^{-1/2}$. In absence of sufficient tie strands, the crystalline phase may not transform to undergo any plastic deformation.

When entangling chains act like tie strands, the LBS density can increase significantly, as depicted in Fig. 4(a). Because $\psi_{intesph}$ includes entangling chains, it can increase with applied rate and decrease with temperature. Admittedly, our description lacks concrete information in the sense that we know little about either the actual values of ψ_{tie} and $\psi_{intersph}$ or contributions from entangling chains. But we do know through Eq. (7) that any crystallization resulting in increased l_{tie} reduces $\psi_{tie}.$ For example, isothermal crystallization at high temperatures may produce longer tie strands, i.e., higher $N_{tie}.$ When crystallization is very slow, much slower than the reptation time, an initial lamella can be significantly thicker, and a free chain may attach onto the seeding crystal after overcoming entanglement. These two factors clearly favor a higher $N_{tie}.$ On the contrary, when fast crystallization minimizes

¹ Since pullout is a concept previously used by us to refer to disengagement of a chain from its network (sliding at junctions) in glassy non-crystalline polymers that may lead to structural failure and brittle breakdown, we differentiate drawing out of lamellae from chain pullout from a chain network in amorphous state of a glassy polymer, by calling this drawing out "pull-out", i.e., adding a hyphen between pull and out. Pull-out occurs when a stem in a lamella is displaced to move relative neighboring stems in the lamella.

depletion of the chain network, N_{tie} is smaller, and more entangling chains exit in the amorphous phase so that $\psi_{intersph}$ is higher. Experiments indeed demonstrate in 3.1.2 of Paper 1 (this volume, p. 125878) for four different SCPs that a given SCP can be either brittle or ductile depending on how it is prepared, i.e., on the thermal history that affects the path of crystallization, which in turn influences the structure of the CCN in terms of the degrees of connectivity (ψ_{tie} and $\psi_{intersph}$) between crystalline domains.

Brittle failure occurs at interspherulitic boundaries when $\psi_{intersph}$ is sufficiently low. With low $\psi_{intersph}$, an insufficient number of chain pullouts leaves spherulites intact (cf. 3.1.7 of Paper 1 (this volume, p. 125878)), so that little transformation (melting) of spherulites can occur. In absence of adequate lateral contraction of spherulites that requires sufficient chain pull-out, strain amplification described in Eq. (1) is severe, and spherulites start to detach at interstitial boundaries, as implied by the *in situ* POM in 3.1.7.3 of Paper 1 (this volume, p. 125878). Although such a failure usually initiates at interstitial boundaries, the crack may also propagate into spherulites to result in intraspherulitic separation. To reiterate, inability to draw (above T_g) in SCPs implies that the CCN fails. A key mode of structural failure occurs when sparse connecting-strand pull-out does not result in meltdown of the crystalline phase. In other words, lack of drawability occurs when areal densities ψ_{tie} and $\psi_{intersph}$ are not sufficiently high so that amorphous interstitial regions are drawn to failure, leaving the crystalline phase largely intact. PLLA and PHA are such SCPs, hardly drawable, at all temperatures

We admit that it is difficult to estimate the value for $\psi_{intersph}$ from the breaking (fracture) stress σ_b according to the following approximate expression

$$\sigma_{b} = \psi_{intersph} f_{c-p} \tag{8}$$

as the threshold chain pull-out force $f_{\text{C-p}}$ is generally unknown. Independent AFM measurements [42,43] of $f_{\text{C-p}}$ may play an important role and enable us to estimate ψ_{intersph} using Eq. (8). On the other hand, Eq. (8) can already provide some insight concerning how the stress depends on temperature and draw rate. In fact, our discussion in Sections 6 and 7 on the temperature and rate effects implicitly employed the picture discussed here. For example, we indicated higher yield stress at higher rate to arise from higher value of ψ_{intersph} , stemming from the contribution of entangling strands to bear load.

8.2. Ductile-brittle transition (DBT) in SCPs: temperature and rate effects

At the chain level, we can associate the breakup of the CCN with the condition that the crystalline phase is hardly deformed. This occurs when few connecting strands are present in the interstitial boundary. This boundary layer is strained to break because the crystalline phase does not melt. A test chain belonging to the boundary layer is seen to dissociate from the CCN. Disappearance of tie strands can take place in one of at least two ways as illustrated in Fig. 8: A tie strand as part of chain 1 can simply pull out of the lower lamella. A different tie strand (chain 2 in Fig. 8) can withstand large strain of the amorphous region between the two lamellae unless, for example, the upper lamella partially melts down due to collective chain pull-out, involving chains 3 and 4. The simultaneous intra-lamellar sliding of multiple chains (2, 3 and 4), as a form of pull-out, may produce a local meltdown of the upper lamella to release all three chains so that they can no longer behave like tie chains. Here the pull-out of chains 3 and 4 can be caused by their entanglements with other strands belonging to chains 2 and 5 respectively. This scenario is pertinent when the drawing rate is sufficiently high or the temperature T is sufficiently low. After massive pull-out, if recrystallization does not occur fast enough, the CCN could not selfrepair. This could explain the poor drawability of PP involving either lower temperature or high drawing speed (cf. Figs. 12 and 14 in Paper 1 (this volume, p. 125878)).

8.3. Class C SCPs

When classifying SCPs into three groups in Introduction of Paper 1 (this volume, p. 125878), we defined nondrawable SCPs (even above T_g) as class C. PHA and PLLA belong to this class. Upon crystallization, PLLA and PHA show poor drawability even when brought to elevated temperatures close to T_m, as shown in Figs. 8 and 13 of Paper 1 (this volume, p. 125878). Such lack of drawability implies that the CCN is weak either because there is low crystallinity to produce sufficient permanent junctions in the CCN, recalling the contrast between Fig. 2(a) and (a'), which is clearly not the case for PHA and PLLA, or ψ_{intersph} is very low so that insufficient connecting strands are present to undergo pull-out from the crystalline phase. For microscopic reasons yet to be formulated, perhaps related to the fact that the crystallization temperature T_c and T_g are close in these polymers, as shown in Table 2 of Paper 1 (this volume, p. 125878), the crystallization in class C SCPs does not take place fast enough to lock up the chain network. In contrast, in PE and PP, the chain network locks up when crystallization occurs everywhere to compete for available (e.g., amorphous) chains, enlisting them into lamellar formation and limiting the removal of interchain crossing (so that there is enough entanglement associated with mutual chain uncrossability).

To improve mechanical characteristics of non-drawable class C SCPs, either effective nucleating agents can be developed and introduced as additives or affine-like pre-melt extension can be carried out, followed by vitrification to preserve the effect of pre-melt extension. Thanks to slow crystallization kinetics and higher T_g than room temperature, elastic pre-melt-stretching can be achieved for PLLA, leading to nanocrystalline PLLA with superior ductility and strength, as shown in Section 11. In contrast, we have little success with PHA: In absence of effective nucleating agents, we have not yet figured out how to establish a robust CCN by controlling the crystallization of PHA.

8.4. Correlation between drawability and crystalline chain mobility

Ultra-high drawability in SCPs has been correlated [67] with polymers that are crystal-mobile (associated with alpha relaxation). It remains unclear whether chain mobility in lamellae dictates the crystal mechanics that in turn influence the structure of the CCN. Separately, there is no detailed understanding of how crystalline alpha relaxation affects the plastic deformation of crystalline phases through chain pull-out, leading to melting and subsequent recrystallization. A recent MD simulation starts to explore such a connection [23]. Perhaps lack of crystalline chain mobility hinders crystal melting and recrystallization. We know that PE cannot draw at high crystallinity and PP loses drawability when spherulites are sufficiently large. Crystalline PLA is hardly drawable above Tg. These examples point to the need to specify the global structural and dynamic characteristics associated with the properties of the CCN. While CCN is a most important object to specify, we lack a basic picture of what a CCN looks like in the sense of what factors determine its structure and strength, characterized at the test chain level, e.g., by N_{fie} (cf. Fig. 1(e) and Eq. (7)) and $f_{\text{c-p}}$.

In conclusion, we have only considered extension of interstitial layers such as those denoted by the white lines in Fig. 1(b) and ignored any shear [54] between spherulites that take place for certain orientations of interspherulitic boundaries, e.g., those denoted by the red (color online) lines. We trust that the pertinent events leading to non-drawability are those associated with interstitial failure due to excessive extension of the interspherulitic layers, highlighted by the white lines in Fig. 1(b). The POM observations (cf. 3.17 of Paper 1 (this volume, p. 125878)) appear to support this simplified view.

9. Responses of glassy SCPs

Non-crystalline glassy polymers usually turn from ductile to brittle upon increase of the drawing speed. In this case, the physics is clearer — the brittle-ductile transition (BDT) in glassy polymers can be understood

as follows [4]. Below the BDT temperature T_{BD} , chain pullout from the (amorphous) chain network takes place to cause localized structural breakdown before global molecular activation, making it impossible to attain macroscopic plastic deformation. Above T_{BD} , the chain network can fulfill the task of activating the glassy state without structural collapse, i.e., without whole-chain pullout. The BDT in glassy polymers with respect to the applied rate can be complicated in the sense that the rate dependence may not be monotonic [68].

Amorphous PET with crystallization is a glassy SCP that is brittle at room temperature (cf. Fig. 4(d) in Paper 1 (this volume, p. 125878)). We infer that crystallization disrupts the original chain network so that the CCN is not as structurally robust as the chain network of the noncrystalline glassy state. Stems in lamellae hardly participate in displacement - we expect chain pull-out in the crystalline phase to be preceded by pullout of amorphous chains from junctions formed by pairs of hairpins in amorphous regions. In general, we expect glassy SCPs to be naturally less ductile in comparison to their amorphous counterparts because crystallization depletes chain entanglement. Moreover, crystalline strands (i.e., stems in lamellae) of the CCN are immobile. During drawing, connecting strands (e.g., entangling chain 1, tie strands 2 and 3) plus bridging strands 4 and 5 in Fig. 3 may pull out from lamellae, causing fragmentation of the crystalline phase: in the glassy state recrystallization cannot occur. Thus, brittle fracture is rather unsurprising to encounter in glassy SCPs. SCPs including ccPET, ccPLLA and PP are all brittle when drawn below T_g (see Figs. 4(d), 8 and 10 in Paper 1 (this volume, p. 125878)).

Even poly(ethylene vinyl alcohol) (EVA) with $T_g=55\,^{\circ}\mathrm{C}$ is brittle unless it is prepared by fast quenching, as shown Fig. 4(c) of Paper 1 (this volume, p. 125878). As in other cases in 3.1.2 of Paper 1 (this volume, p. 125878), the resulting CCN can be significantly affected by how crystallization takes place. The effect of crystallization on ductility is generally detrimental for glassy SCPs: Amorphous PET is ductile while crystalline PET is not; PP is usually brittle in its glassy state; a certain way to crystallize EVA produces ductile EVA while another method of crystallization makes EVA brittle at room temperature.

10. Mechanical improvement through predrawing

For SCPs that are drawable, i.e., ductile in their rubbery state (above Tg), the effect of predrawing can be demonstrated. Here predrawing refers to extension of crystalline SCPs at temperature T satisfying T_m > T > Tg, and PP offers a particularly interesting and well-known example [65,69-71]. In a simpler case, it was discovered that melt-stretching can turn brittle PS completely ductile at room temperature [72-76]. Affine-like pre-melt-stretching changes the structure of the chain network through the effect of geometric condensation [76,77] to influence the ability of a glassy amorphous polymer to undergo yielding. Predrawing can produce a similar effect in SCPs. In fact, the important role of tie strands in driving a glassy SCP to undergo yielding can be demonstrated by examining the predrawing effect. In other words, uniaxial predrawing is an attractive way to alter the areal density of tie strands in a predrawn SCP so that it gains ductility after predrawing. Biaxial orientation of PP (BOPP) below T_m is a commonly applied industrial strategy to make PP useable below freezing. The situation could be different if crystallization minimally disrupts the chain networking. PE shows its BDT [78] at -196 °C, well below T_g, because of the fast crystallization that traps the existing entanglement in molten state. If an SCP can be induced to crystallize only on nanoscales so as not to disrupt the chain network, e.g., by having crystallization sites densely distributed on a subchain scale, it may be ductile in its glassy state. This scenario is discussed in the following Section 11.

Separately, can predrawing also improve ductility and mechanical strength of SCPs such as PP above T_g ? To answer this question, it is necessary to envision how predrawing of SCPs change the crystalline morphology and chain networking, which is a key topic of this Section. We speculate based on the available phenomenology [41] as well as

emerging evidence from a recent molecular dynamics simulation [61] of fast melt-stretching that upon large plastic deformation in tensile extension, some recrystallization could result in a crystalline state as shown in Fig. 9(a). For example, during necking, the folded chain crystals (lamellae) may be predominantly converted into extended chain crystals (ECCs), e.g., from Figs. 8 to 9(a), which is a view that is also suggested by Zuo et al. [22]. In this ECC, most LBSs such as chain 2 having their two dangling strands may be embedded in the ECC. The ECC reflects geometric condensation of LBSs in the altered CCN, corresponding to increased ψ_{tie} . These effects could make a predrawn glassy SCP ductile, i.e., capable of yielding. Such a predrawing effect has been explored in Section 3.3 of Paper 1 (this volume, p. 125878).

Past in situ X-ray studies [22,48–50] have shown the effect of predrawing above T_g on the crystalline morphology of SCPs. While Fig. 9(a) depicts an extreme form of the final CCN, a more common perception [22] of the resulting states may look like the cartoon in Fig. 9(b) where lamellae include those that are remnants and others that are due to recrystallization. The predrawing can be expected to result in either geometric condensation or dilation of the CCN, i.e., the effect shown in Fig. 9(b) can be represented or depicted as shown in Fig. 9(c), depending on whether the drawing is carried out along the original predrawing direction (Z axis) or perpendicular to Z axis along either X or Y axis.

To understand the origin of the high strength $\sigma_{predw(b)}$ observed from the extension of predrawn PP at room temperature in Fig. 17(b) in 3.3.1 of Paper 1 (this volume, p. 125878), we estimate the magnitude of $f_{c\cdot p}$ in an LBS for pull-out from the crystalline phase that causes the predrawing to terminate in failure. Specifically, we evaluate the lower bound $f_{c\cdot p(min)}$ of chain tension by considering the limit where the increased ψ_{tie} (by geometric condensation) is as high as ϕ of Eq. (5). This amounts to setting α in Eq. (7) and Fig. 7 to unity so that

$$\sigma_{\text{predw}(b)} = \varphi f_{\text{c-p(min)}}.\tag{9}$$

Taking p=0.29 nm and $l_{\rm K}=1.0$ nm as characteristic values [45] for PP, at breaking (due to chain pull-out) we have $\sigma_{\rm predw}\sim 320$ MPa according to Fig. 17(b) in Paper 1 (this volume, p. 125878). Thus, Eq. (9) yields $f_{\rm c-p(min)}\sim 93$ pN. Thus we expect a threshold chain pull-out force $f_{\rm c-p}>f_{\rm c-p(min)}=93$ pN in the case of PP. Recent AFM measurements of SCPs suggest [79] that $f_{\rm c-p}$ ranges from tens of pN to one thousand pN.

We can conversely estimate the areal density of the load-bearing chains across adjacent spherulites in an undrawn PP in terms of the yield stress level. Assuming yielding is caused by chain pull-out from lamellae, we have, in terms of Eq. (9).

Taking $\sigma_y\sim 30$ MPa, we have $\psi_{intersph}/\phi<30/300=0.1,$ given $\sigma_{predraw(b)}=300$ MPa. Since interstitial boundaries do not all line up perpendicular to the drawing direction (cf. Fig. 1(b)), $\psi_{intersph}<0.1\phi$ is an under-estimate of $\psi_{intersph}$. In other words, for PP, the load-bearing strand density $\psi_{intersph}$ connecting adjacent spherulites, may be on the order of 0.1ϕ .

According to the recent AFM measurements [44] the pull-out force shows logarithmic rate dependence. Since yield stress also has logarithmic dependence on the applied rate, the above assertion to relate yielding to chain pull-out from lamella seems reasonable.

Since PP [80,81] loses ductility below their T_g , it is interesting to show how predrawing affects the ductility in their glassy states. At $-20\,^{\circ}$ C, Fig. 17(c) in Paper 1 (this volume, p. 125878) reveals that after predrawing PP is highly ductile, with its specific work of fracture increasing by a factor of thirty. Apparently, the predrawing has produced geometric condensation (demonstrated in Fig. 9(c)) that promotes activation in glassy state. It is presumably the increased ability (by geometric condensation) to produce molecular mobility that permits morphological rearrangement without premature failure of the CCN. The ductility is achieved despite the cavities produced by the predrawing at room temperature.

Thus, indeed, predrawing can make PP much stronger over a wider range of temperature, spanning across T_g : The tensile strength of the

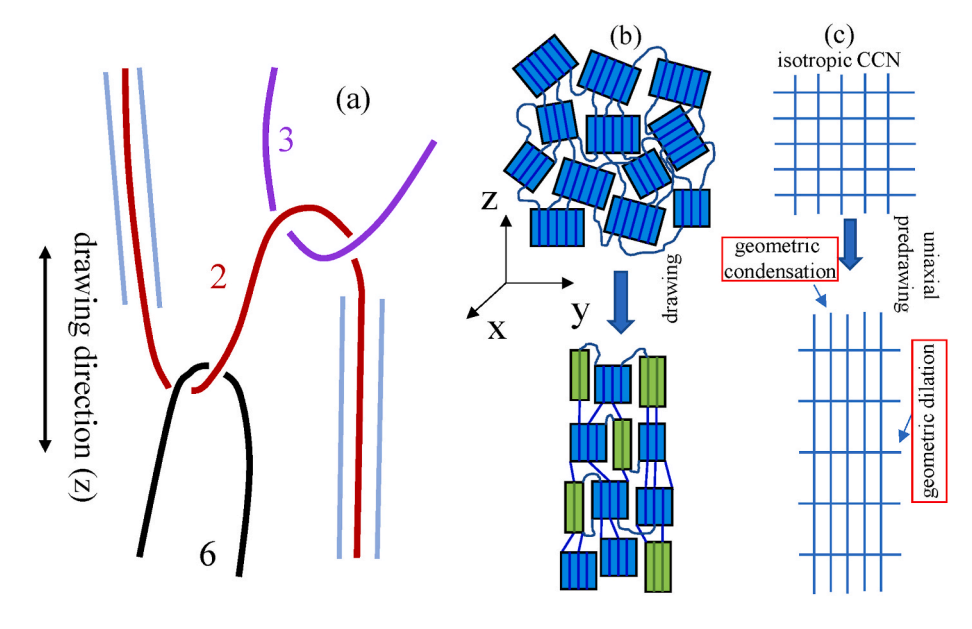


Fig. 9. (a) Extended chain crystalline state. (b) Transformation of crystalline phase where green (color online) lamellae are from recrystallization, and the blue crystals are from the original lamellae. (c) Geometric condensation (XY plane) – when drawn along Z axis and dilation (XZ and YZ planes) – when drawn along X or Y axis of the CCN (crystalline features omitted) during uniaxial drawing where dots representing crystalline domains are omitted for simplicity. (For interpretation of the references to color in this figure legend, the reader is referred to the Web version of this article.)

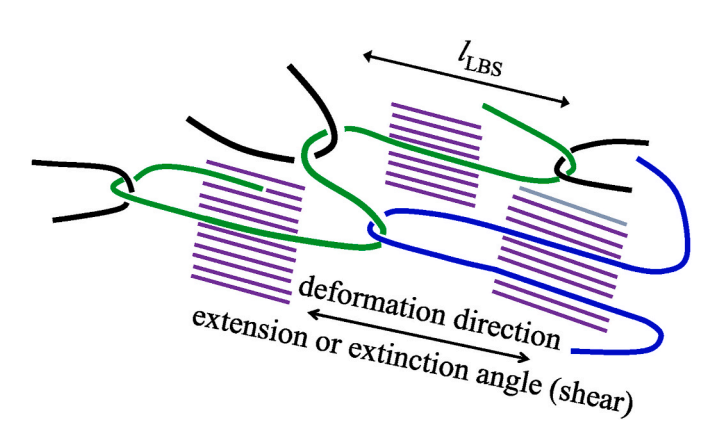


Fig. 10. Pre-melt-stretching induced nano-confined crystallization (NCC) where fully stretched load-bearing strands (LBSs) act as nucleating sites.

predrawn PP is very high at room temperature, exhibiting a stress level considerably higher than that displayed by isotropic glassy polymers during their ductile drawing. In contrast, as shown in Fig. 13 of Ref. [76], commercial PC shows a yield stress level of 55 MPa (instead of 300 MPa) and draws in a ductile manner to $\lambda_{DR}=2.3$ at room temperature until failure to true stress of 140 ca. MPa, substantially lower than 300 MPa displayed by predrawn PP.

11. Pre-melt-stretching to induce nano-confined crystallization in class B SCPs

For class B SCPs whose non-crystalline state is accessible, such as PLLA and PET, the effect of pre-melt deformation is easier to describe in absence of the structural complication due to crystallization. According to the preceding discussions in Section 9, brittle fracture is ordinarily inevitable in untreated glassy SCPs. In other words, it is essentially improbable to avoid pull-out-induced molecular holes from growing into macroscopic cracks in glassy SCPs made of space-filling spherulites of appreciable size. In PET and PLLA crystallization takes place rather slowly with nucleation sites sparsely distributed. Chains move over long distances to join large lamellae in sizable spherulites. In such a crystallization process, chain entanglement can be severely disrupted, resulting in a weak CCN.

On the other hand, readily accessible non-crystalline forms of class B

SCPs can be exploited to acquire geometric condensation and crystallization that retain chain entanglement. In other words, we envision scenarios that result in a creation of a super tough, heat resistant (i.e., having high heat distortion temperature) and optically transparent SCPs with utilization temperature up to $T_{\rm m}$.

Specifically, for class B SCPs such as PLLA and PET, we can contemplate a well-controlled way to induce nano-confined crystallization (NCC) by pre-melt-stretching at temperature $T_{ms} > T_g$. It is well known [41] that melts of high molecular weight can be elastically extended to a substantial stretching ratio λ_{ms} , e.g., 3, without encountering significant chain disentanglement that produces structural failures of various kinds during melt stretching [82]. We can carry out elastic (i.e., affine like) melt stretching to produce sufficient chain orientation and induce crystallization. This pre-stretching effect can be retained by quenching the pre-stretched class B SCP to room temperature (below T_g). Depending on the stretching ratio λ_{ms} and crystallization kinetics, cold crystallization may or may not have taken place before the termination of melt-stretching, as demonstrated in Section 3.4 of Paper 1 (this volume, p. 125878). Both procedures may accomplish the objective of stretching-induced cold nano-crystallization [83, 141]

Stretched entanglement strands in the chain network, as shown in Fig. 10, can be expected to be precursors for cold crystallization either upon annealing of the quenched pre-melt-stretched sample at $\rm T_{ann}>T_{g}$ or during stress relaxation from melt stretching. Because of the uncrossability constraint, in this elastic stretching limit, the crystallization would be confined to the length scale of an average network's mesh size $l_{\rm LBS}$, as depicted in Fig. 10. In other words, chains do not travel beyond the scale of $l_{\rm LBS}$ before crystallization. The NCC rapidly traps the entanglement. The pin-down of the chain network ensures that crystalline domains are nanoscopic, on the scale of $l_{\rm LBS}$ in all directions.

Stretched strands can act to induce crystallization that would not occur otherwise in the isotropic state within the experimental time scale. Since there is plausibly a Gaussian distribution for the mesh size l_{LBS} , as illustrated in Fig. 11, at a given stretching ratio λ_{ms} , only a fraction of shorter strands in the distribution are effectively extended. In the affine deformation limit, a strand of length $N_c = (\lambda_{ms})^2$ can be straightened because λ_{ms} is given by the chain contour length divided by its coil size: $(N_c)^{1/2}$. Longer strands in the shade under the curve in Fig. 11 would remain coiled and make no contribution as precursors for cold crystallization. Instead, they become incorporated into the cold crystallization by attaching to their adjacent straightened strands. Since straightened LBSs in the unshaded part of the distribution in Fig. 11 are numerous and

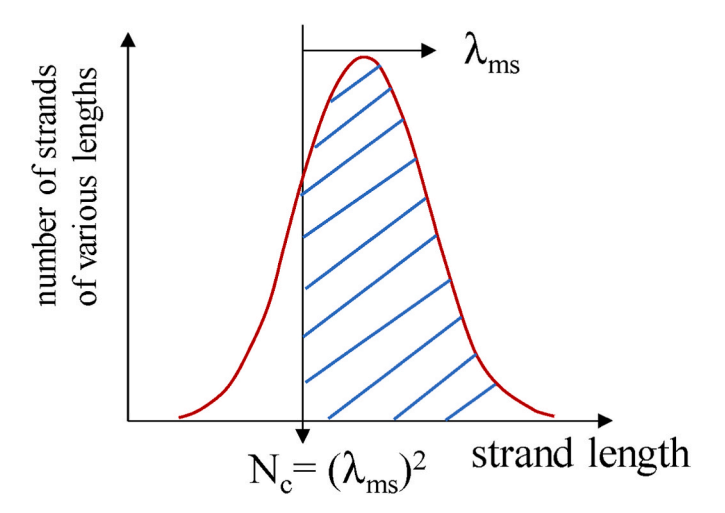


Fig. 11. Distribution of strand lengths in the CCN where strands belonging to the shaded region cannot undergo NCC upon melt stretching to λ_{ms} , while strands with length shorter than N_c in the unshaded portion of the distribution may participate in NCC.

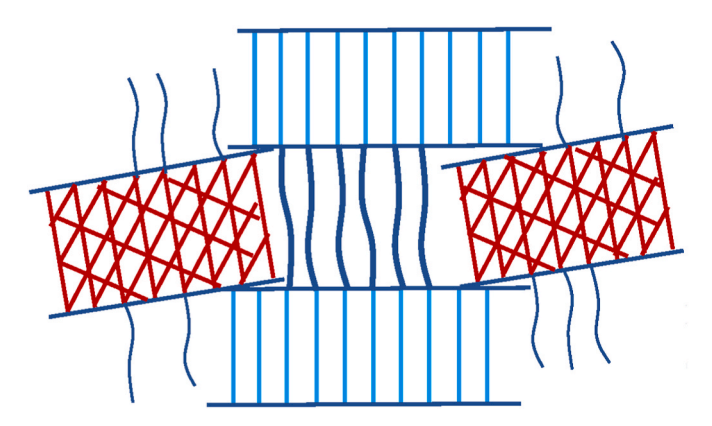


Fig. 12. Shrinkage of shaded crystals in the amorphous region through melting to allow unjamming so that stretched tie strands produce observed retractive stress during annealing of significantly predrawn SCPs.

spatially uniformly distributed on nanoscopic length scales, the induced crystals (shish-kebabs) may not grow beyond on the scale of l_{LBS} , which may be 10 nm, as each growing crystal competes to enlist long strands from their surroundings. For a higher value of λ_{ms} , the vertical dividing line moves toward the right-hand side in Fig. 11, showing a larger (unshaded) population of straightened strands. Consequently, the density of crystals may increase, and the crystal sizes may decrease with increasing λ_{ms} due to the reduced population of yet-to-crystallize strands.

The preceding discussion pertains to cold crystallization in a premelt-stretched class B SCP in absence of ongoing stretching. We can also consider a case where the polymer is subjected to continuous uniaxial extension in a wide range of rates at $T_{ms} > T_g$ until failure (cf. Fig. 27 of Paper 1 (this volume, p. 125878)). It is plausible that in presence of crystallization at T_{ms} not too far above T_g further cold crystallization can take place beyond a stretching ratio $\lambda_{ms}(T_{ms},\dot{\epsilon})$. Such crystallization may act to constrain the chain network, making it easier for the non-crystalline strands to stretch and to become the nuclei for new crystal formation.

In conclusion, if an SCP in its non-crystalline state can be fast meltdeformed, it may have a chance to develop NCC that can avoid depletion of chain entanglement. Either quiescent cold crystallization in premelt-deformed SCPs or cold crystallization during melt-deformation can produce such a crystalline state. They are optically clear and highly stable against heat because of the NCC. Two prominent commercial polymers, PLLA and PET, are ideal candidates for this scenario of stretch-induced NCC to materialize, because both of them can be quenched from their molten states into glassy amorphous state without encountering any discernible crystallization. It turns out that for PLLA and PET, after melt-stretching ten degrees above Tg, cold crystallization can occur in minutes. In contrast, in the isotropic state, it takes hours for them to cold crystallize because of low segmental mobility. In passing, we also acknowledge that NCC can also occur from pre-shear instead of pre-extension. However, since simple shear does not produce geometric condensation, ductility does not improve after NCC [84]. Moreover, the NCC forming mechanism of course applies to biaxial stretching. In fact, Mylar is simply PET with NCC produced by biaxial melt stretching, i.e., Mylar is BOPET.

12. Mechanical melting

The effect of predrawing can also be examined by annealing. Upon unloading after predrawing, a specimen slightly retracts until the crystalline domains jam up so that the CCN is in significant internal tension. After storage at room temperature, upon annealing above the predrawing temperature but below $T_{\rm m}$, depending on the annealing temperature $T_{\rm ann}$ and degree of predrawing (which is a function of the predrawing temperature, draw ratio, and drawing rate), we can expect the strained CCN to show retractive stress. In other words, at temperatures above the predrawing temperature, force imbalance can take place with the available retractive forces in stretched LBSs exceeding $f_{\rm c-p}(T)$ from crystalline phase. When the annealing occurs under constraint, e. g., while keeping the predrawing specimen at fixed length, retractive stress emerges as shown in 3.3.1.3 of Paper 1 (this volume, p. 125878).

Such emergence of retractive stress implies that crystal jamming is partially removed. As depicted in Fig. 12, melting of shaded crystals in (red color online) would reduce jamming, allowing tie strands (thick dark lines) to cause the retraction of the CCN. As expected (cf. Fig. 19 of Paper 1 (this volume, p. 125878)), at sufficiently high temperatures, e. g., 90 °C and above, the rising retractive stress is followed by a decline whose magnitude increases with temperature. This steep stress decrease implies massive pull-out of the LBSs from crystalline domains, rendering fewer LBSs contributing to the remaining retractive stress. Thus, the mechanically induced melting during annealing, activated by holding the predrawn specimen fixed in length (along the direction of predrawing) occurs in two steps, (a) preliminary melting leading to slight shrinkage of crystals in amorphous interstitial regions (presumably due to some level of chain pull-out – no melting can take place without pullout) so that only the holding force at the two ends of the specimens balances the retractive stress in the CCN; (b) subsequent massive tie strand pull-out occurs if Tann is high enough, causing the growing retractive stress to decline over time. Here pull-out occurs because the retractive intrachain tension exceeds the threshold f_{c-p} , which can be expected to vanish near T_m.

The phenomenon shown in Fig. 19 in Paper 1 (this volume, p. 125878) reminds us of the same behavior that we termed *elastic yielding*, observed [85] of a predrawn glassy polymer upon annealing above the predrawing temperature but still well below T_g that significant retractive stress emerges. The vitrification plays a similar role to crystallization in SCPs: Upon unloading (well below T_g), a small amount of retraction occurs in a predrawn glassy polymer. Subsequently, the predrawn specimen ceases to retract to indicate a force balance between intrachain tension and intersegmental forces. Upon annealing, the intersegmental forces weaken, leading to force imbalance, which is macroscopically observed as emergence of retractive stress. In the same spirit, the mechanical melting is elastic yielding as yielding of SCPs is caused by the embedded elastic chain tension.

The mechanical melting phenomenon has two important implications. First, it directly supports the concept of CCN as the underlying global structure in an SCP. Second, it points to the effect of processing in

predrawn SCPs: existence of internal retractive stress.

13. Summary

SCPs manifests the following mechanical characteristics. (1) Creep test shows above T_g and below T_m that the system is "crosslinked" by the crystalline phase so that the solid state has finite cohesion whose magnitude depends on both areal density of load-bearing strands (e.g., tie strands) and the forces required for chain pull-out from the crystalline phase (2) Brittle failure of SCPs (e.g., PHB and PLLA, even PE at high crystallinity). above T_g indicates that the crystallization can result in a structurally weakened CCN, incapable of causing the crystalline phase to yield and undergo plastic deformation. In principle, there are two types of failure of the CCN, either substantial crystalline phase breaks down without recrystallization or few chain pull-outs from crystals (due to lack of sufficient tie strands) take place, leaving the crystalline phase intact and forcing detachment between crystalline and amorphous phases. (3) Glassy SCPs tend to be brittle because (a) the CCN is usually less robust relative to the chain network before crystallization (b) crystalline segments of a chain do not participate in activation of the glassy state. (4) Fast crystallizing SCPs such as PE and PP are the best example and strongest support for the concept that a robust CCN ensures outstanding mechanical characteristics. The fast crystallization avoids depletion of chain entanglement so that there are sufficient tie strands to permit transformation (i.e., plastic deformation) of the crystalline phase (spherulites and lamellae). On the other hand, a quantitative description of just how crystallization depletes entanglement is still missing. Moreover, when the degree of undercooling is varied, different morphologies tend to result, adding complexity in the study of the effect of crystallization on mechanical responses. We cannot rule out that the dependence of the mechanical responses on crystallization history in Section 3.1.2 of Paper 1 (this volume, p. 125878) is not largely due to the resulting morphological difference where the leading consequence is described by Eq 1.

Although we have acquired some conceptual understanding of the molecular mechanism for ductility in SCPs, we are far from having a quantitative description of either the structure of the CCN in terms of the areal densities of connecting (tie and entangling) strands or mechanics of the CCN (e.g., the role of connecting strands for crystalline transformation) as a function of temperature. However, we are certain that a robust CCN means existence of sufficient connecting strands and a resilient CCN is necessary for ductility of SCPs. An adequate CCN amounts to every chain participating in many crystalline domains, i.e., there are many crystalline and amorphous subchains within a test chain as depicted in Fig. 1(e). While tie strands are necessary for crystal melting, structural integrity requires entangling strands (e.g., strand b in Fig. 1(d) and chain 1 in Fig. 3) to be numerous as an indication that the chain network is preserved during crystallization. High drawability in the post-yield regime may require sufficiently fast recrystallization to retain enough crystallinity that must be present as "crosslinkers" for SCPs above T_o.

The present discussion is only concerned with leading order effects, i. e., mechanical deformation under isothermal conditions. In reality, there can be significant viscous heating [41] upon yielding. Since we are mostly concerned about the lack of ductility and drawability, the post-yield viscous heating is not a central effect to investigate and is therefore neglected there. In this work we have only presented a qualitative rationale for temperature and rate effects that show opposing trends for different SCPs, as indicated in Sections 6.2 and 7. We did not discuss mechanical response of SCPs to (uniaxial) compression where shape-change is realized in a different way. The contrast is well known for brittle glassy polymers such as PS and PMMA of high molecular weight: While brittle in tension they are ductile in compression [86]. Similarly, brittle or nondrawable SCPs of high molecular weight can be expected to be ductile in compression either above or below $T_{\rm g}$. It is at least interesting to ask whether compression results in fracture for SCPs

of low molecular weight that do not form a CCN. We have carried out uniaxial compression of PEO of $M_{\rm w}=2000~{\rm g/mol}$ at room temperature and found, data omitted, the cylindrical specimen to fracture upon large compression, in agreement with our expectation: CCN is necessary even in compression of SCPs above $T_{\rm g}.$

In conclusion, the concept of CCN allows us to emphasize the essential role of chain networking through interchain uncrossability. In other words, we have gone beyond the mere mention of the concept of polymer entanglement, which has been vaguely invoked frequency in the literature on mechanical behavior of SCPs. We envision the role of CCN to be explicit and direct in terms of the mechanical outcome: SCPs are ductile only when there is a robust CCN to enable transformation of the crystalline phase while retaining sufficient crystallinity for them to behave like viscoelastic solids. It is the crystalline process that dictates the structure of the CCN. Various experiments in Paper 1 (this volume, p. 125878) show how thermal history and pre-deformation influence the construction of the CCN and determine the nature of mechanical responses. Since the central theme of the present work is to investigate the origin of ductility and lack of drawability, we have omitted the phenomenological Maxwell-model-like account [17,53] of ductile responses of SCPs.

Funding

This work is supported, in part, by the Polymers program at the National Science Foundation (DMR1905870 and DMR2210184) as well as ACS-PRF 60897-ND. We greatly appreciate the constructive comments from four reviewers that significantly improved the manuscript.

CRediT authorship contribution statement

Shi-Qing Wang: Supervision, Conceptualization, Methodology, Formal analysis, Validation, Writing – original draft, Writing – review & editing. Travis Smith: Data curation, Methodology, Formal analysis, Validation, Writing – review & editing. Chaitanya Gupta: Data curation, Methodology, Formal analysis, Validation, Writing – review & editing. Asal Y. Siavoshani: Data curation, Formal analysis.

Declaration of competing interest

The authors declare that they have no known competing financial interests or personal relationships that could have appeared to influence the work reported in this paper.

Data availability

Data will be made available on request.

References

- I.M. Ward, J. Sweeney, Mechanical Properties of Solid Polymers, 3rd, John Wiley & Sons, Ltd., Chichester, UK, 2012.
- [2] I.M. Ward, Structure and Properties of Oriented Polymers, Springer Science & Business Media. 2012.
- [3] A.S. Argon, The Physics of Deformation and Fracture of Polymers, Cambridge University Press, 2013.
- [4] S.-Q. Wang, S. Cheng, P. Lin, X. Li, A phenomenological molecular model for yielding and brittle-ductile transition of polymer glasses, J. Chem. Phys. 141 (9) (2014), 094905.
- [5] M. Razavi, S. Cheng, D. Huang, S. Zhang, S.-Q. Wang, Crazing and yielding in glassy polymers of high molecular weight, Polymer 197 (2020), 122445.
- [6] G. Williamson, B. Wright, R. Haward, The preparation and properties of fractions from high density polyethylenes, J. Appl. Chem. 14 (3) (1964) 131–140.
- [7] S.H. Cho, R.A. Register, Minimum molecular weight and tie molecule content for ductility in polyethylenes of varying crystallinity, Macromolecules 55 (8) (2022) 3249–3258.
- [8] R. Seguela, Critical review of the molecular topology of semicrystalline polymers: the origin and assessment of intercrystalline tie molecules and chain entanglements, J. Polym. Sci. B Polym. Phys. 43 (14) (2005) 1729–1748.

- [9] L. Mandelkern, F.L. Smith, M. Failla, M.A. Kennedy, A.J. Peacock, The brittle-ductile transition in linear polyethylene, J. Polym. Sci. Pt. B-Polym. Phys. 31 (4) (1993) 491–493.
- [10] A. Peterlin, Molecular model of drawing polyethylene and polypropylene, J. Mater. Sci. 6 (6) (1971) 490–508.
- [11] P.J. Flory, D.Y. Yoon, Molecular morphology in semi-crystalline polymers, Nature 272 (5650) (1978) 226–229.
- [12] A. Keller, D. Pope, Identification of structural processes in deformation of oriented polyethylene, J. Mater. Sci. 6 (6) (1971) 453–478.
- [13] F. Nilsson, X. Lan, T. Gkourmpis, M.S. Hedenqvist, U.W. Gedde, Modelling tie chains and trapped entanglements in polyethylene, Polymer 53 (16) (2012) 3504–3601
- [14] A. Keller, Unusual orientation phenomena in polyethylene interpreted in terms of the morphology, J. Polym. Sci. 15 (79) (1955) 31–49.
- [15] J. Schultz, Microstructural aspects of failure in semicrystalline polymers, Polym. Eng. Sci. 24 (10) (1984) 770–785.
- [16] B.A. Schrauwen, R.P. Janssen, L.E. Govaert, H.E. Meijer, Intrinsic deformation behavior of semicrystalline polymers, Macromolecules 37 (16) (2004) 6069–6078.
- [17] R. Hiss, S. Hobeika, C. Lynn, G. Strobl, Network stretching, slip processes, and fragmentation of crystallites during uniaxial drawing of polyethylene and related copolymers, A compar. stud., Macromol. 32 (13) (1999) 4390–4403.
- [18] K. Iwata, Role of entanglement in crystalline polymers 1. Basic theory, Polymer 43 (24) (2002) 6609–6626.
- [19] C. Luo, J.-U. Sommer, Frozen topology: Entanglements control nucleation and crystallization in polymers, Phys. Rev. Lett. 112 (19) (2014), 195702.
- [20] C. Luo, J.-U. Sommer, Role of thermal history and entanglement related thickness selection in polymer crystallization, ACS Macro Lett. 5 (1) (2016) 30–34.
- [21] V. Litvinov, R. Deblieck, C. Clair, W. Van Den Fonteyne, A. Lallam, R. Kleppinger, D.A. Ivanov, M.E. Ries, M. Boerakker, Molecular structure, phase composition, melting behavior, and chain entanglements in the amorphous phase of highdensity polyethylenes, Macromolecules 53 (13) (2020) 5418–5433.
- [22] F. Zuo, J.K. Keum, X. Chen, B.S. Hsiao, H. Chen, S.-Y. Lai, R. Wevers, J. Li, The role of interlamellar chain entanglement in deformation-induced structure changes during uniaxial stretching of isotactic polypropylene, Polymer 48 (23) (2007) 6867–6880.
- [23] R. Ranganathan, V. Kumar, A.L. Brayton, M. Kroger, G.C. Rutledge, Atomistic modeling of plastic deformation in semicrystalline polyethylene: role of interphase topology, entanglements, and chain dynamics, Macromolecules 53 (12) (2020) 4605–4617.
- [24] H.D. Keith, F.J. Padden Jr., R.G. Vadimsky, Intercrystalline links in polyethylene crystallized from the melt, J. Polym. Sci. 2 Polym. Phys. 4 (2) (1966) 267–281.
- [25] A. Lustiger, R.L. Markham, Importance of tie molecules in preventing polyethylene fracture under long-term loading conditions, Polymer 24 (12) (1983) 1647–1654.
- [26] Y.-L. Huang, N. Brown, Dependence of slow crack growth in polyethylene on butyl branch density: morphology and theory, J. Polym. Sci. B Polym. Phys. 29 (1) (1991) 129–137.
- [27] R.S. Porter, L.-H. Wang, Uniaxial extension and order development in flexible chain polymers, J. Macromol. Sci., Part C 35 (1) (1995) 63–115.
- [28] M. Ishikawa, K. Ushui, Y. Kondo, K. Hatada, S. Gima, Effect of tie molecules on the craze strength of polypropylene, Polymer 37 (24) (1996) 5375–5379.
- [29] K.-H. Nitta, M. Takayanagi, Role of tie molecules in the yielding deformation of isotactic polypropylene, J. Polym. Sci. B Polym. Phys. 37 (4) (1999) 357–368.
- [30] Z. Spitalsky, T. Bleha, Elastic moduli of highly stretched tie molecules in solid polyethylene, Polymer 44 (5) (2003) 1603–1611.
- [31] Y.F. Men, J. Rieger, G. Strobl, Role of the entangled amorphous network in tensile deformation of semicrystalline polymers, Phys. Rev. Lett. 91 (9) (2003) 4.
- [32] S. Lee, G.C. Rutledge, Plastic deformation of semicrystalline polyethylene by molecular simulation, Macromolecules 44 (8) (2011) 3096–3108.
- [33] J.M. Kim, R. Locker, G.C. Rutledge, Plastic deformation of semicrystalline polyethylene under extension, compression, and shear using molecular dynamics simulation, Macromolecules 47 (7) (2014) 2515–2528.
- [34] I.-C. Yeh, J.L. Lenhart, G.C. Rutledge, J.W. Andzelm, Molecular dynamics simulation of the effects of layer thickness and chain tilt on tensile deformation mechanisms of semicrystalline polyethylene, Macromolecules 50 (4) (2017) 1700–1712.
- [35] P.A. Olsson, E. Andreasson, E. Bergvall, E.P. Jutemar, V. Petersson, G.C. Rutledge, M. Kroon, All-atomic and coarse-grained molecular dynamics investigation of deformation in semi-crystalline lamellar polyethylene, Polymer 153 (2018) 305–316.
- [36] Y. Lu, Y. Wang, R. Chen, J. Zhao, Z. Jiang, Y. Men, Cavitation in isotactic polypropylene at large strains during tensile deformation at elevated temperatures, Macromolecules 48 (16) (2015) 5799–5806.
- [37] A. Pawlak, A. Galeski, A. Rozanski, Cavitation during deformation of semicrystalline polymers, Prog. Polym. Sci. 39 (5) (2014) 921–958.
- [38] A. Rozanski, A. Krajenta, R. Idczak, A. Galeski, Physical state of the amorphous phase of polypropylene-influence on free volume and cavitation phenomenon, J. Polym. Sci. B Polym. Phys. 54 (5) (2016) 531–543.
- [39] A. Pawlak, A. Galeski, Cavitation during tensile drawing of annealed high density polyethylene, Polymer 51 (24) (2010) 5771–5779.
- [40] A. Pawlak, A. Galeski, Plastic deformation of crystalline polymers: the role of cavitation and crystal plasticity, Macromolecules 38 (23) (2005) 9688–9697.
- [41] S.-Q. Wang, Nonlinear Polymer Rheology: Macroscopic Phenomenology and Molecular Foundation, Wiley, Hoboken, NJ, 2018.
- [42] Y. Song, P. Yang, K. Jiang, W. Zhang, Force-induced melting of a single polyethylene oxide chain from single crystal: molecular behavior and influencing factors, Polym. Crystal. 2 (2) (2019), e10048.

[43] Z. Ma, P. Yang, X. Zhang, K. Jiang, Y. Song, W. Zhang, Quantifying the chain folding in polymer single crystals by single-molecule force spectroscopy, ACS Macro Lett. 8 (9) (2019) 1194–1199.

- [44] P. Yang, Y. Song, W. Feng, W. Zhang, Unfolding of a single polymer chain from the single crystal by air-phase single-molecule force spectroscopy: toward better force precision and more accurate description of molecular behaviors, Macromolecules 51 (18) (2018) 7052–7060.
- [45] L.J. Fetters, D.J. Lohse, D. Richter, T.A. Witten, A. Zirkel, Connection between polymer molecular-weight, density, chain dimensions, and melt viscoelastic properties, Macromolecules 27 (17) (1994) 4639–4647.
- [46] S.-Q. Wang, On chain statistics and entanglement of flexible linear polymer melts, Macromolecules 40 (24) (2007) 8684–8694.
- [47] K. Chen, K.S. Schweizer, Theory of relaxation and elasticity in polymer glasses, J. Chem. Phys. 126 (1) (2007), 014904.
- [48] M.F. Butler, A.M. Donald, W. Bras, G.R. Mant, G.E. Derbyshire, A.J. Ryan, A real-time simultaneous small- and wide-angle X-ray scattering study of in-situ deformation of isotropic polyethylene, Macromolecules 28 (19) (1995) 6382-6303
- [49] X. Chen, F. Lv, F. Su, Y. Ji, L. Meng, C. Wan, Y. Lin, X. Li, L. Li, Deformation mechanism of iPP under uniaxial stretching over a wide temperature range: an insitu synchrotron radiation SAXS/WAXS study, Polymer 118 (2017) 12–21.
- [50] F. Lv, X. Chen, C. Wan, F. Su, Y. Ji, Y. Lin, X. Li, L. Li, Deformation of ultrahigh molecular weight polyethylene precursor fiber: crystal slip with or without melting, Macromolecules 50 (17) (2017) 6385–6395.
- [51] W. Wu, G. Wignall, L. Mandelkern, A SANS study of the plastic deformation mechanism in polyethylene, Polymer 33 (19) (1992) 4137–4140.
- [52] Z. Ma, C. Shao, X. Wang, B. Zhao, X. Li, H. An, T. Yan, Z. Li, L. Li, Critical stress for drawing-induced α crystal–mesophase transition in isotactic polypropylene, Polymer 50 (12) (2009) 2706–2715.
- [53] Y. Men, Critical Strains Determine the Tensile Deformation Mechanism in Semicrystalline Polymers, ACS Publications, 2020, pp. 9155–9157.
- [54] A. Galeski, Strength and toughness of crystalline polymer systems, Prog. Polym. Sci. 28 (12) (2003) 1643–1699.
- [55] K. Schmidt-Rohr, H.W. Spiess, Chain diffusion between crystalline and amorphous regions in polyethylene detected by 2D exchange carbon-13 NMR, Macromolecules 24 (19) (1991) 5288–5293.
- [56] J.F. Mano, Cooperativity in the crystalline α-relaxation of polyethylene, Macromolecules 34 (26) (2001) 8825–8828.
- [57] J.D. Ferry, Viscoelastic Properties of Polymers, Wiley, New York, 1980.
- [58] S.-Q. Wang, S. Cheng, Experiments-inspired molecular modeling of yielding and failure of polymer glasses under large deformation, Chapter 12, in: C. Roth (Ed.), Polymer Glasses, CPC Press, 2016.
- [59] A.Y. Malkin, C.J.S. Petrie, Some conditions for rupture of polymer liquids in extension, J. Rheol. 41 (1) (1997) 1–25.
- [60] Y. Wang, S.-Q. Wang, Rupture in rapid uniaxial extension of linear entangled melts, Rheol. Acta 49 (11–12) (2010) 1179–1185.
- [61] Y. Zheng, M. Tsige, S.Q. Wang, Molecular dynamics simulation of entangled melts at high rates: identifying entanglement lockup mechanism leading to true strain hardening, Macromol. Rapid Commun. (2022), 2200159.
- [62] R.H. Boyd, Relaxation processes in crystalline polymers: experimental behaviour — a review, Polymer 26 (3) (1985) 323–347.
- [63] R.H. Boyd, Relaxation processes in crystalline polymers: molecular interpretation — a review, Polymer 26 (8) (1985) 1123–1133.
- [64] B.E. Read, Mechanical relaxation in isotactic polypropylene, Polymer 30 (8) (1989) 1439–1445.
- [65] I.H. Hall, The effect of temperature and strain rate on the stress-strain curve of oriented isotactic polypropylene, J. Polym. Sci. Polym. Chem. 54 (160) (1961) 505–522.
- [66] L.H. Sperling, Introduction to Physical Polymer Science, John Wiley & Sons, 2005.
- [67] W.G. Hu, K. Schmidt-Rohr, Polymer ultradrawability: the crucial role of α-relaxation chain mobility in the crystallites, Acta Polym. 50 (8) (1999) 271–285.
- [68] X. Li, S.-Q. Wang, Mapping brittle and ductile behaviors of polymeric glasses under large extension, ACS Macro Lett. 4 (10) (2015) 1110–1113.
- [69] A.J. de Vries, Structure and properties of uni- and biaxially oriented polypropylene films: Part I - structural characterization, Pure Appl. Chem. 53 (5) (1981) 1011–1037.
- [70] A.J. de Vries, Structure and properties of uni- and biaxially oriented polypropylene films: Part 2 - mechanical and other end-use properties, Pure Appl. Chem. 54 (3) (1982) 647–670.
- [71] S. Yoshida, T. Sawada, T. Kawamura, K. Nitta, Molecular orientation behavior of isotactic polypropylene films under uniaxial and biaxial deformation at elevated temperatures, Int. Polym. Process. 27 (2) (2012) 237–244.
- [72] G. Gruenwald, Mod. Plast. 38 (1960) 137.
- [73] D.H. Ender, R.D. Andrews, Cold drawing of glassy polystyrene under dead load, J. Appl. Phys. 36 (10) (1965) 3057–3062.
- [74] C.B. Bucknall, Toughened plastics, Springer (1977).
- [75] Y. Tanabe, H. Kanetsuna, Brittle-to-ductile transition based upon amorphous orientation of polystyrene monofilaments, J. Appl. Polym. Sci. 22 (9) (1978) 2707–2711.
- [76] G.D. Zartman, S. Cheng, X. Li, F. Lin, M.L. Becker, S.-Q. Wang, How melt-stretching affects mechanical behavior of polymer glasses, Macromolecules 45 (16) (2012) 6719–6732.
- [77] G. Liu, H. Sun, S. Rangou, K. Ntetsikas, A. Avgeropoulos, S.-Q. Wang, Studying the origin of "strain hardening": basic difference between extension and shear, J. Rheol. 57 (1) (2012) 89–104.

- [78] P.I. Vincent, A correlation between critical tensile strength and polymer crosssectional area, Polymer 13 (12) (1972) 558–560.
- [79] Y. Song, Z. Ma, P. Yang, X. Zhang, X. Lyu, K. Jiang, W. Zhang, Single-molecule force spectroscopy study on force-induced melting in polymer single crystals: the chain conformation matters, Macromolecules 52 (3) (2019) 1327–1333.
- [80] A. Van der Wal, J. Mulder, H. Thijs, R. Gaymans, Fracture of polypropylene: 1. The effect of molecular weight and temperature at low and high test speed, Polymer 39 (22) (1998) 5467–5475.
- [81] A. van der Wal, J.J. Mulder, R.J. Gaymans, Fracture of polypropylene: 2. The effect of crystallinity, Polymer 39 (22) (1998) 5477–5481.
- [82] X. Zhu, S.-Q. Wang, Mechanisms for different failure modes in startup uniaxial extension: tensile (rupture-like) failure and necking, J. Rheol. 57 (1) (2012) 223–248.
- [83] M. Razavi, W. Zhang, H.A. Khonakdar, A. Janke, L. Li, S.-Q. Wang, Inducing nanoconfined crystallization in PLLA and PET by elastic melt stretching, Soft Matter 17 (6) (2021) 1457–1462.
- [84] T. Smith, J. Feng, L. Zou, M. Gao, M. Prévôt, S.Q. Wang, Nano-confined crystallization in poly (lactic acid)(PLA) and poly (ethylene terephthalate)(PET) induced by various forms of pre-melt-deformation, Macromol. Rapid Commun. (2022), 2200293.
- [85] S. Cheng, S.-Q. Wang, Elastic yielding after cold drawing of ductile polymer glasses, Macromolecules 47 (11) (2014) 3661–3671.
- [86] J. Liu, P. Lin, S. Cheng, W. Wang, J.W. Mays, S.-Q. Wang, Polystyrene glasses under compression: ductile and brittle responses, ACS Macro Lett. 4 (10) (2015) 1072–1076